Energy cascade for distribution and evolution of supermassive black holes

Zhijie Xu (zhijie.xu@pnnl.gov)
zhijie.xu@pnnl.gov https://orcid.org/0000-0003-0459-4531

Article

Keywords: Supermassive black hole, Coevolution, Mass accretion, Energy cascade

Posted Date: January 11th, 2023

DOI: https://doi.org/10.21203/rs.3.rs-2465508/v1

Additional Declarations: There is **NO** Competing Interest.

Vol. **000**, 1–10 (2022) Preprint 7 January 2023 Compiled using LaTeX style file v3.0

Energy cascade for distribution and evolution of supermassive black holes

Zhijie (Jay) Xu,[1]★
[1]*Physical and Computational Sciences Directorate, Pacific Northwest National Laboratory; Richland, WA 99352, USA*

Accepted XXX. Received YYY; in original form ZZZ

ABSTRACT

Strong correlations exist between supermassive black holes (SMBHs) and their host galaxies. These correlations suggest a missing component in our current understanding: the role of energy cascade in SMBH-bulge coevolution. In this picture, energy is continuously cascaded from bulge scale r_b down to the BH scale (Schwarzschild radius r_s). Energy cascade has a scale-independent, but decreasing rate $\varepsilon_b(t) \approx \sigma_b^3/r_b$ due to the cooling of baryonic component, where σ_b is bulge velocity dispersion. The bulge mass-size (M_b-r_b) relation can be expressed as $M_b \propto \varepsilon_b^{2/3} r_b^{5/3} G^{-1}$, or a bulge density-size relation $\rho_b \propto \varepsilon_b^{2/3} r_b^{-4/3} G^{-1}$, with $\varepsilon_b \approx a^{-5/2} \times 10^{-4} m^2/s^3$, as confirmed by the galaxy survey, where a is the scale factor and G is the gravitational constant. Intermediate length scales can be defined based on the dominant physics on that scale, i.e. the BH sphere of influence r_B, radiation scale r_p, and dissipation scale r_x. For SMBH with a mass M_B, bolometric luminosity L_B, energy cascade leads to a "cascade" force that must be balanced by the BH radiation force in its early life, i.e. $L_B/c = M_B\varepsilon_b/\sigma_p$, where c is light speed and σ_p is the velocity dispersion on scale r_p. Since ε_b is much larger in the early universe, BH accretion can be super-Eddington with L_B exceeding the Eddington limit. In addition, the BH mass-dispersion relation ($M_B \propto \sigma_b^5$) is a natural result of the cascade theory. By introducing two dimensionless parameters $\gamma = L_B/(M_B\varepsilon_b)$ and $\eta = (GL_B/c^5)^{1/4}$, the distribution and evolution of SMBHs can all be mapped onto the γ-η plane. By setting $r_s \leqslant r_p \leqslant r_B$, the upper limit of distribution is found to be $L_B \propto (\varepsilon_b M_B)^{4/5} G^{-1/5} c$. The lower limit is found to be $L_B \propto (\varepsilon_b M_B)^{4/3} G^{1/3} c^{-5/3}$. Quasars tend to approach the upper limit, while dormant SMBHs (Sgr A* and M31) tend to approach the lower limit. A three stage mathematical model is proposed for SMBH evolution involving co-evolution, transitional, and dormant stages, respectively. Models are finally compared against the BH accretion history from quasar luminosity function from 2dF Redshift Survey, local galaxy and SMBHs data, and high redshift quasars from SDSS DR7 and CFHQS surveys.

Key words: Supermassive black hole; Coevolution; Mass accretion; Energy cascade;

CONTENTS

1 INTRODUCTION

Supermassive black holes (SMBHs) are ubiquitously associated with the center of massive galaxies that contain bulges (Kormendy & Ho 2013). Numerous observations demonstrate strong correlations between SMBHs and their host galaxies at such a fundamental level that we believe the two are "co-evolving". The earliest black hole demography involves the correlation between SMBH mass M_B and bulge luminosity L_b (Magorrian et al. 1998; Marconi & Hunt 2003; Graham & Scott 2013; McConnell & Ma 2013). Since the bulge mass M_b is related to the bulge luminosity L_b, the M_B-L_b correlation strongly hints direct correlation between two masses M_B and M_b. Bulge mass can be directly derived using the virial theorem (i.e. $M_b \propto r_b\sigma_b^2$, where r_b and σ_b are the bulge size and velocity dispersion) or from dynamical modeling. The M_B-M_b correlation is generally consistent with a linear relation $M_B \propto M_b$ (Magorrian et al. 1998; Marconi & Hunt 2003; Haring & Rix 2004). A more tighter correlation with the smallest intrinsic scatter was discovered for SMBH mass and bulge dispersion (M_B-σ_b). This provides the strongest evidence of a fundamental relationship between SMBHs and their host galaxies (Ferrarese & Merritt 2000; Merritt & Ferrarese 2001; Hopkins et al. 2007; Hu 2008; Gultekin et al. 2009a; McConnell & Ma 2013). Many studies suggest a power law scaling $M_B \propto \sigma_b^\alpha$ with $\alpha \approx 5$. Examples are $\alpha = 4.8$ (Ferrarese & Merritt 2000), $\alpha = 4.86$ (Ferrarese & Ford 2005), $\alpha = 5.4$ (Marsden et al. 2020), $\alpha = 5$ (Woo et al. 2015), $\alpha = 4.24$ (Gultekin et al. 2009a), and $\alpha = 4$ or 4.5 (Hu 2008).

Currently, the physical mechanisms responsible for these tight correlations are not completely understood. This is partially because of the huge disparity in scales from black holes ($\sim 10^{-3}$pc) to their host galaxies ($\sim$10kpc), and the complex physics involved on black hole

★ E-mail: zhijie.xu@pnnl.gov; zhijiexu@hotmail.com

and bulge scales. Various mechanisms were proposed to interpret these tight correlations. A possible mechanism involves the SMBH feedback during its active galactic nucleus (AGN) phase, where significant amount of energy/momentum is injected into surrounding gas. The released energy or momentum unbind the surrounding gas, prevent the star formation, and shape the evolution of host galaxy (Silk & Rees 1998; King 2003). An alternative mechanism proposes the co-evolution is established through same source of gas supply provided for both black holes mass accretion and the star formation (Menci et al. 2016). A statistical interpretation is also presented such that the tight correlation is just a consequence of statistical convergence during hierarchical formation of galaxy structure (Peng 2007). Recent study using both observational data and hydrodynamic simulations provides more support for the AGN feedback as the responsible mechanism (Ding et al. 2020).

From observed SMBH-bulge correlations, a very interesting finding is: if we combine the M_B-σ_b correlation ($M_B \propto \sigma_b^5$), the linear correlation $M_B \propto M_b$, and the virial theorem $M_b \propto r_b\sigma_b^2$ together, we arrive at a simple relation $\sigma_b^3/r_b = Const$. This is particularly interesting as we know that

$$\epsilon_b = \sigma_b^3/r_b = \sigma_b^2/(r_b/\sigma_b) \tag{1}$$

is the rate of energy cascade in bulge, where kinetic energy σ_b^2 on scale r_b is cascaded in a turnaround time r_b/σ_b. Since energy cascade is a well-established concept in turbulence theory, this suggests a quick revisit of some fundamental ideas of turbulence.

Turbulence consists of a random eddies (building blocks of turbulence) on different length scales that are interacting with each other. The classical picture of turbulence is an eddy-mediated cascade process, where kinetic energy is injected on large scale, cascaded by eddies of different scales, and dissipated by viscosity on the smallest scale. Energy of large eddies feeds smaller eddies, which feeds even smaller eddies, and so on to the smallest scale η where viscous dissipation is dominant (Richardson 1922). Provided the Reynolds number is high enough, there exists a range of length scales where the viscous force is negligible and the inertial force is dominant (inertial range). The rate of energy passing down the cascade (ε unit:m^2/s^3) is scale-independent in the inertial range that is related to the eddy velocity u and eddy scale l as $\varepsilon \propto u^3/l$ (same as Eq. (1)). This rate matches exactly the rate of energy dissipation due to viscosity ν at the smallest scale η, below which the viscous dissipation is dominant over inertial effect (the dissipation range). The dissipation scale

$$\eta = (\nu^3/\varepsilon)^{1/4} \tag{2}$$

is determined by ε and the fluid viscosity ν (Kolmogorov 1941).

Go back to SMBH-bulge system, we choose correlations (Ferrarese & Ford 2005; Marconi & Hunt 2003)

$$\frac{M_B}{10^8 M_\odot} = 1.66\left(\frac{\sigma_b}{200km/s}\right)^{4.86}, \qquad M_B \approx 0.002 M_b \quad \text{and} \quad M_b \approx 3 r_b \sigma_b^2/G, \tag{3}$$

which leads to a rate of energy cascade $\varepsilon_b = \sigma_b^3/r_b \approx 10^{-4} m^2/s^3$, comparable to the local galaxy data in Table A1.

The strong correlations found between SMBHs and host galaxies suggest the existence of energy cascade in SMBH-bulge system (see Eq. (1)), which will be discussed in Section 3. Figure 1 provides a schematic plot of the energy cascade in a SMBH-bulge system with bulge mass M_b, BH mass M_B, and BH bolometric luminosity L_B. Energy is injected on the bulge scale with a rate of $\varepsilon_b M_b$, cascaded down to the black hole scale with a scale independent rate ε_b. The injected energy is dissipated on small scales through viscous gas, the radiation from star formation in bulge, and the luminosity of black holes L_B. Which dissipation is dominant depends on the stage of SMBH evolution. All relevant scales for SMBH evolution are also presented. The radiation pressure from BH luminosity L_B should balance the "cascade" pressure P_r due to the turbulent motion and energy cascade in surrounding gases. All relevant data for this work can be found at Zenodo.org (Xu 2022a).

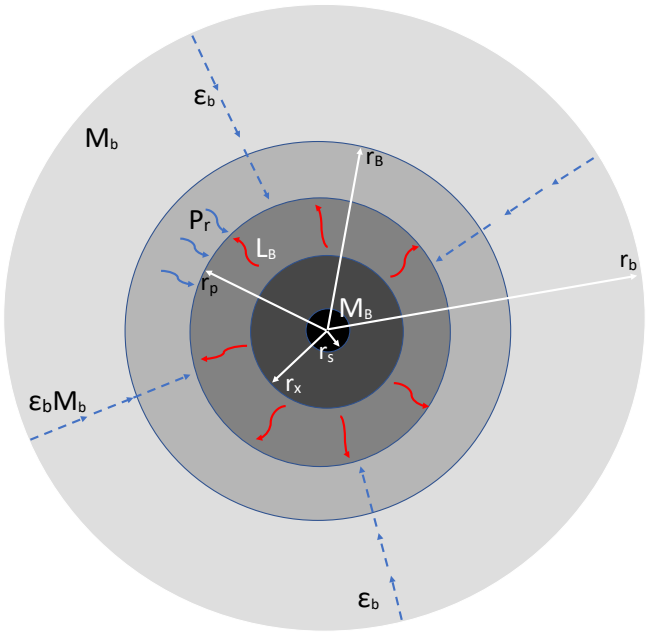

Figure 1. Schematic plot of the SMBH-bulge system with bulge mass M_b, BH mass M_B, and BH bolometric luminosity L_B. Five relevant length scales are also shown, i.e. the bulge scale r_b (Eq. (15)), the BH sphere of influence r_B (Eq. (15)), the radiation scale r_p (Eq. (16)), the dissipation scale r_x (Eq. (17)), and the Schwarzschild radius r_s (Eq. (15)). Energy is continuously cascaded from bulge scale down to the BH scale with a scale-independent rate ε_b. Energy cascade leads to a "cascade" force (or pressure P_r) that must be balanced by the BH radiation (see Eqs. (10) and (59)) such that super-Eddington accretion is possible. With $r_s \leqslant r_p \leqslant r_B$, the upper and lower limits of SMBH distribution can be rigorously developed (Eqs. (24) and (26)).

2 ENERGY CASCADE IN DARK MATTER FLOW

When self-gravitating collisionless dark matter flow in an expanding background is concerned, the energy evolution can be described by a cosmic energy equation (Irvine 1961; Layzer 1963),

$$\frac{\partial E_y}{\partial t} + H\left(2K_p + P_y\right) = 0, \tag{4}$$

which is a manifestation of energy conservation in expanding background. Here K_p is the specific (peculiar) kinetic energy, P_y is the specific potential energy in physical coordinate, $E_y = K_p + P_y$ is the total energy, $H = \dot{a}/a$ is the Hubble parameter, and a is the scale factor. The cosmic energy equation (4) admits a power-law solution of $K_p \propto t$ and $P_y \propto t$ such that a constant rate of energy production ε_u can be defined by $K_p = -\varepsilon_u t$,

$$\varepsilon_u = -\frac{K_p}{t} = -\frac{3}{2}\frac{u^2}{t} = -\frac{3}{2}\frac{u_0^2}{t_0} = -\frac{9}{4}H_0 u_0^2 \approx -4.6\times10^{-7}\frac{m^2}{s^3}, \tag{5}$$

where $u_0 \equiv u\,(t = t_0) \approx 355 km/s$ is the one-dimensional velocity dispersion of dark matter from N-body simulation (see dataset Xu

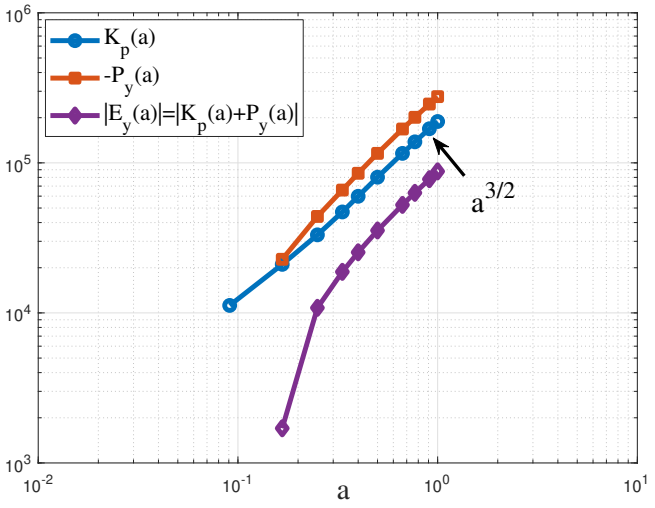

Figure 2. The time variation of specific kinetic and potential energies (km^2/s^2) from N-body simulation. Both exhibit power-law scaling with scale factor textita, i.e. $K_p\ (a) \propto a^{3/2} \propto t$ and $P_y\ (a) \propto a^{3/2} \propto t$. The proportional constant $\boldsymbol{\varepsilon_u}$ can be estimated in Eq. (5).

2022a). Here t_0 is the physical time at present epoch. The negative ε_u reflects the inverse cascade of kinetic energy from small to large scales. Figure 2 plots the time variation of kinetic and potential energy from a dark matter only N-body simulation by Virgo consortium (Frenk et al. 2000).

Hydrodynamic turbulence can be freely decaying. A good example is to stir the coffee-milk and let it freely mix. The energy injected is gradually dissipated at a certain rate ε. However, the dark matter flow seems to be freely growing, with increasing kinetic energy from the releasing of gravitational potential. Therefore, the constant ε_u stands for the rate of (specific) kinetic energy increase (Eq. (5)). It also has a profound physical meaning as the rate of energy cascade across different scales that is independent of both time and scales.

Scaling laws on small scale (less than the typical halo size) can be identified for the flow of dark matter (Xu 2022b). On small scale, the kinetic energy v_r^2 on scale r should follow a two-thirds law

$$v_r^2 \propto (-\varepsilon_u)^{2/3} r^{2/3}. \tag{6}$$

The two-thirds law in Eq. (6) can be equivalently written as,

$$-\varepsilon_u \propto \frac{v_r^2}{r/v_r} = \frac{v_r^3}{r}. \tag{7}$$

Equation (7) (similar to Eq. (1)) describes the cascade in dark matter, where the kinetic energy v_r^2 on scale r is cascaded to large scale during a turnaround time of $t_r = r/v_r$. Combining Eq. (6) with the virial theorem $Gm_r/r \propto v_r^2$ on scale r, the typical mass m_r (enclosed within r) and density ρ_r are all determined by ε_u, G, and r:

$$m_r = \alpha_r \varepsilon_u^{2/3} G^{-1} r^{5/3} \quad \text{and} \quad \rho_r = \beta_r \varepsilon_u^{2/3} G^{-1} r^{-4/3}, \tag{8}$$

where α_r and β_r are two constants. The predicted four-thirds law $\rho_r(r) \propto r^{-4/3}$ for mean halo density enclosed in scale r can be compared against galaxy rotation curves (see Fig. 3), with $\alpha_r \approx 5.28$ and $\beta_r = \alpha_r/(4\pi/3) \approx 1.26$ for the best fitting.

3 ENERGY CASCADE IN DYNAMICS OF BULGE

Baryons dominate the mass of matter at center of galaxies. Galaxies were formed by dissipation of the baryonic component within collisionless dark matter halos (White & Rees 1978). There exists a certain range of scales where the dynamics of baryons might be well approximated by self-gravitating collisionless flow, but with a different rate of energy cascade ϵ_b. For interstellar medium with a typical kinematic viscosity of $\nu = 10^{16} m^2/s$ (Parker 1958), the dissipation scale $\eta_d = (\nu^3/\epsilon_b) \approx 10^{-7}$kpc (see Eq. (2)) with $\epsilon_b \approx 10^{-4} m^2/s^3$ at $z = 0$ (Table A1). For scales $r \gg \eta_d$, the dissipation can be neglected and dynamics of baryons can be approximately self-gravitating collisionless, but with a rate of cascade $\epsilon_b \equiv \epsilon_b(a)$ decreasing with time due to the cooling (dissipation) of baryonic component. By contrast, the rate of energy cascade ε_u in dark matter is a constant of time (Eq. (5)). Therefore, similar to the scaling laws in dark matter (Eqs. (7) and (8)), we can write the mass and density of baryons on scale r,

$$m_r = \alpha_r \varepsilon_b^{2/3} G^{-1} r^{5/3} \quad \text{and} \quad \rho_r = \beta_r \varepsilon_b^{2/3} G^{-1} r^{-4/3}. \tag{9}$$

The time scale, velocity dispersion v_r^2, cascade pressure P_r due to the random motion, and the cascade force F_r on scale r read

$$\begin{aligned} &t_r \propto \varepsilon_u^{-1/3} r^{2/3}, \quad v_r^2 = \gamma_r G m_r/r = \alpha_r \gamma_r (\varepsilon_b r)^{2/3}, \\ &P_r = \rho_r v_r^2 = \alpha_r \beta_r \gamma_r \varepsilon_b^{4/3} G^{-1} r^{-2/3}, \\ &F_r = 4\pi r^2 P_r = 4\pi \alpha_r \beta_r \gamma_r \varepsilon_b^{4/3} G^{-1} r^{4/3} = 3 v_r^4/(\gamma_r G), \end{aligned} \tag{10}$$

where $\gamma_r < 1$ is a numerical constant with $\gamma_r \approx 1/3$ for galaxy bulge (Marconi & Hunt 2003). The cascade pressure P_r comes from the velocity dispersion to balance the gravity. For dissipationless flow like collisionless dark matter, we should also have

$$\varepsilon_b m_r \propto \dot{m}_r v_r^2 \propto G m_r \dot{m}_r/r \quad \text{and} \quad \dot{m}_r \propto \varepsilon_b G^{-1} r, \tag{11}$$

where $\varepsilon_b m_r$ is the rate of energy injection into scale r and $\dot{m}_r = m_r/t_r$ is the average rate of mass flow into the scale r. This is good for small luminosity L_B or large scale r, where the dissipation effect by SMBH can be neglected. For entire bulge, the rate of energy injection is about $\varepsilon_b M_b$, where M_b is the bulge mass (Fig. 1).

We first check the scaling laws in Eq. (9). The 5/3 scaling between bulge mass and size ($m_r \propto r^{5/3}$ or $r \propto {m_r}^{0.6}$) is supported by many studies, especially for early-type galaxies (ETGs). These studies show a galaxy mass-size relation $r \propto M^\alpha$ with $\alpha \approx$ [0.5 0.6] (Huertas-Company et al. 2013), $\alpha \approx 0.6$ (Mowla et al. 2019a), and $\alpha \approx 0.55$ (Shen et al. 2003). By contrast, we predict $\alpha = 0.6$ from Eq. (9). The -4/3 scaling between density and size ($\rho_r \propto r^{-4/3}$) can also be verified by the galaxy data. Figure 3 presents the predicted -4/3 scaling law for dark matter halo core density ρ_s with scale radius r_s that can be extracted from galaxy rotation curves. Two different density models (NFW and pISO or Pseudo-isothermal) are applied to extract the dark matter halo density. The same scaling law is also confirmed for galaxy bulge density $\rho_b = M_b/(4\pi r_b^3/3)$ varying with the bulge size r_b. Data is taken from galaxy survey in Table A1.

Next, we will determine the time-dependence of cascade rate ϵ_b. Dynamics on bulge scale satisfies (from Eq. (7) and by definition):

$$\varepsilon_b = \frac{\sigma_b^3}{r_b} \propto -\frac{d}{dt}\left(\sigma_b^2\right), \tag{12}$$

where the rate of cascade ε_b represents the rate of energy change. Here σ_b is the velocity dispersion on bulge scale and r_b is the size of bulge. In this work, we use the effective radii r_e that contains half of the total light and the effective stellar velocity dispersion σ_e at r_e, i.e $\sigma_b = \sigma_e$ and $r_b = r_e$ (Marconi & Hunt 2003). Let's assume on bulge scale, there exists a general relation $\sigma_b^2 r_b^n = Const$ in the statistically steady state of bulge dynamics, where n is an exponent to be determined from observational data. Combined this relation

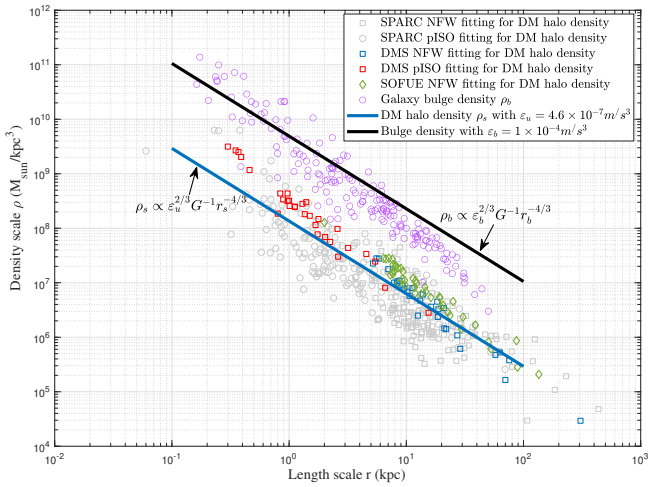

Figure 3. The predicted -4/3 law for variation of density ρ with scale r. Three sources are used for dark matter halos: i) SPARC (Spitzer Photometry & Accurate Rotation Curves) including 175 late-type galaxies (Lelli et al. 2016; Li et al. 2020); ii) DMS (DiskMass Survey) including 30 spiral galaxies (Martinsson et al. 2013); iii) SOFUE (compiled by Sofue) with 43 galaxies (Sofue 2016). Good agreement confirms the existence of energy cascade with a rate ε_u in dark matter halos. The same scaling also exists between bulge density ρ_b and size r_b, where data is taken from Table A1. This confirms the existence of energy cascade in bulge with a rate ε_b.

with dynamics in Eq. (12) and the virial relation $\sigma_b^2 \propto GM_b/r_b$, the evolution of all relevant quantities on bulge scale should read

$$\begin{aligned} &r_b \propto a^{\frac{3}{2+n}}, \quad \sigma_b \propto a^{-\frac{3n}{4+2n}}, \quad M_b \propto a^{\frac{3-3n}{2+n}}, \quad \dot{M}_b \propto a^{-\frac{9n}{4+2n}} \\ &\rho_b \propto a^{-3}, \quad \varepsilon_b \propto a^{-\frac{6+9n}{4+2n}}, \quad r_M \propto a^{\frac{6+9n}{10+5n}}, \end{aligned} \tag{13}$$

where M_b is the mass of bulge. Here r_M is the bulge size for a fixed bulge mass M_b at different redshift (see Eq. (9)). From the redshift evolution of galaxy mass-size relation, a power-law is usually observed with $r_M \propto (1+z)^{-\alpha} \propto a^{\alpha}$ with $\alpha \approx 1$, especially for the early type galaxies (ETGs). This is supported by studies with $\alpha \approx 1.01$ (Huertas-Company et al. 2013), $\alpha \approx 1.05$ (Yang et al. 2020), and $\alpha \approx 0.95$ (Mowla et al. 2019b). With $\alpha = 1$, we expect $n = 1$ from Eq. (13), bulge mass $M_b \propto lna$, bulge size $r_b \propto a$, and dispersion $\sigma_b^2 \propto a^{-1}$ (due to cooling of baryonic component). The rate of bulge energy cascade should finally read (from Eq. (13))

$$\varepsilon_b \approx \varepsilon_0 a^{-5/2}, \tag{14}$$

with an average rate $\varepsilon_0 \approx 10^{-4} m^2/s^3$ at $z = 0$ (see Table A1). For comparison, sun has a mass-to-light ratio of 5122 kg/W or an equivalent energy dissipation rate of $2\times10^{-4} m^2/s^3$, which is on the same order as the average energy cascade rate in bulge.

4 LENGTH SCALES FOR SMBH EVOLUTION

For SMBH evolution, six physical quantities are directly involved: the bulge mass M_b, black hole bolometric luminosity L_B, black hole mass M_B, scale-independent rate of energy cascade ε_b, plus two constants: the gravitational constants G and light speed c. In this description, there exists an energy cascade with a rate ε_b from the scale of bulge down to the scale of BH, where energy is dissipated into radiation. The energy cascade across multiple scales facilitates the energy exchange between the host galaxy and SMBH.

In addition, SMBH has three effects on the host galaxy: i) the gravitational effect through G and BH mass M_B; ii) the feedback through radiation (involving c and luminosity L_B); iii) the dissipation effect through dissipating the cascaded energy (involving constants G, c, and ε_b). These effects lead to critical length scales that are determined by the dominant physics on relevant scales. The first two scales are the size of bulge r_b and the sphere of influence of black hole r_B, both of which are determined by the energy cascade and the mass on that scale (Eq. (9)). The smallest scale is the Schwarzschild radius r_s. Therefore, three length scales (from large to small) read:

$$\begin{aligned} r_b &= (1/\alpha_r)^{3/5} M_b^{3/5} G^{3/5} \varepsilon_b^{-2/5} \\ r_B &= (1/\alpha_r)^{3/5} M_B^{3/5} G^{3/5} \varepsilon_b^{-2/5} \quad \text{and} \quad r_s = 2GM_B/c^2. \end{aligned} \tag{15}$$

The fourth length scale r_p can be determined by combining the black hole feedback with the energy cascade. Since the radiation pressure due to BH luminosity is $P_{rad} = L_B/(4\pi r^2 c)$, the radiation scale r_p can be obtained by setting $P_{rad} = P_r$ in Eq. (10) such that

$$r_p = \left(\frac{GL_B}{3\alpha_r^2 \gamma_r c}\right)^{\frac{3}{4}} \varepsilon_b^{-1}. \tag{16}$$

Radiation pressure is dominant below scale r_p. At r_p, the radiation pressure equals the turbulence cascade pressure to balance the gravity from all scales above r_p.

The fifth length scale r_x can be determined by the dissipation effect of black hole and the energy cascade,

$$r_x = \left(\frac{\nu_B^3}{\varepsilon_b}\right)^{\frac{1}{4}} = \left(\frac{8 z_r^3 G^3 M_B^3}{c^3 \varepsilon_b}\right)^{\frac{1}{4}}, \tag{17}$$

where $\nu_B = z_r c r_s = 2 z_r G M_B/c$ is an equivalent kinematic viscosity of BH with a numerical constant $z_r \approx 1/3$ from kinetic theory of gases. Table A1 presents the five relevant length scales computed for some SMBHs and their host galaxies.

In addition, three fundamental dimensionless parameters can be obtained from six relevant physical quantities,

$$\beta = \frac{L_B}{M_b \varepsilon_b}, \quad \gamma = \frac{L_B}{M_B \varepsilon_b}, \quad \text{and} \quad \eta = \left(\frac{GL_B}{c^5}\right)^{\frac{1}{4}}. \tag{18}$$

The physical meaning of these dimensionless parameters can be found as the coefficients between black hole luminosity L_B and the mass on different scales using Eq. (11),

$$L_B \propto \gamma \frac{GM_B \dot{M}_B}{r_B} \propto \beta \frac{GM_b \dot{M}_b}{r_b} \quad \text{and} \quad L_B \propto \eta \dot{m}_p c^2, \tag{19}$$

where m_p is the total mass enclosed within scale r_p.

The ratio between different length scales can be conveniently expressed in terms of γ and η:

$$\begin{aligned} &\frac{r_B}{r_s} = \frac{1}{2\alpha_r^{3/5}} \left(\frac{\gamma}{\eta^4}\right)^{\frac{2}{5}}, \quad \frac{r_p}{r_s} = \frac{1}{2(3\alpha_r^2\gamma_r)^{3/4}} \left(\frac{\gamma}{\eta}\right), \\ &\frac{r_B}{r_p} = \frac{(3\alpha_r^2\gamma_r)^{3/4}}{\alpha_r^{3/5}} (\gamma\eta)^{-\frac{3}{5}}, \quad \frac{r_x}{r_s} = \frac{z_r^{3/4}}{2^{1/4}} \left(\frac{\gamma}{\eta^4}\right)^{\frac{1}{4}}, \\ &\frac{r_x}{r_p} = \left(\frac{6 z_r \alpha_r^2 \gamma_r}{\gamma}\right)^{\frac{3}{4}}, \quad \frac{r_x}{r_B} = (2z_r)^{3/4} \alpha_r^{3/5} \left(\frac{\eta^4}{\gamma}\right)^{\frac{3}{20}}. \end{aligned} \tag{20}$$

In addition, relation of mass, size, and velocity dispersion between SMBHs and their host galaxy is

$$\frac{M_B}{M_b} = \frac{\beta}{\gamma} = \left(\frac{\sigma_B}{\sigma_b}\right)^5, \quad \frac{r_B}{r_b} = \left(\frac{\beta}{\gamma}\right)^{\frac{3}{5}}, \quad \frac{\sigma_B}{\sigma_b} = \left(\frac{\beta}{\gamma}\right)^{\frac{1}{5}}. \tag{21}$$

5 SMBH DISTRIBUTION AND EVOLUTION IN γ-η PLANE

The distribution and evolution of SMBHs can be described by η and γ defined in Eq. (18). Figure 4 presents both the distribution of local SMBHs, high-redshift quasars, and the evolution path of a typical SMBH in γ-η plane. All data comes from four different sources:

(i) Table A1 presents a survey of available galaxies with known bulge mass M_b, size r_b, or velocity dispersion σ_b. The rate of energy cascade ε_b can be explicitly calculated from Eq. (12). With the luminosity L_B and BH mass M_B in these galaxies, η and γ can be easily computed by Eq. (18) and plotted in Fig. 4 as square symbols (red for Seyfert galaxies and blue for others).

(ii) The quasar data (mass M_B and luminosity L_B) was obtained from the Sloan Digital Sky Survey Data Release 7 (SDSS DR7) with over 100,000 quasars (Schneider et al. 2010; Shen et al. 2011). Only quasars with redshift $0.26 < z < 0.41$ (gray circles) and $4.01 < z < 4.62$ (black circles) are plotted in Fig. 4. When computing parameters γ for quasars, the rate of energy cascade ε_b is computed by Eq. (14).

(iii) Quasars with high redshift $z \approx 6$ (blue circles in Fig. 4) was obtained from the Canada–France High-z Quasar Survey (CFHQS) (Willott et al. 2010). Here $\varepsilon_b \approx 0.018 m^2/s^3$ at this redshift.

(iv) The evolution of M_B of a typical SMBH is obtained from the history of the average co-moving BH mass density. By assuming the QSO (quasi-stellar object) phase is dominant for BH mass accretion, the evolution of co-moving BH mass density can be estimated from quasar luminosity function from 2dF Redshift Survey (Yu & Tremaine 2002). The green solid line in Fig. 4 presents a representative evolution path of a typical SMBH in γ-η plane, which has a mass $M_0 = 10^9 M_\odot$ at $z = 0$. To map that evolution path onto the γ-η plane, the first step is to compute the luminosity history from mass accretion history of M_B,

$$\frac{L_B}{M_0} = \frac{\dot{M}_B}{M_0}\frac{\epsilon c^2}{1-\epsilon} = \frac{\partial (M_B/M_0)}{\partial a} H_0 a^{-1/2} \frac{\epsilon c^2}{1-\epsilon}, \tag{22}$$

where M_0 is the BH mass at $z = 0$. Here $\epsilon = 0.1$ is the radiative efficiency and $H_0 \approx$70km/s/Mpc is the Hubble constant. With L_B solved from the evolution of M_B in Eq. (22) and ε_b from Eq. (14), the evolution of γ and η can be obtained. Figure 5 plots the time variation of BH mass M_B (normalized by $M_0 = 10^9 M_\odot$) that is derived from the quasar luminosity function from 2dF Redshift Survey (Yu & Tremaine 2002). The BH luminosity L_B (normalized by $L_0 = 4.45 \times 10^{43}$erg/s at $z = 0$) and two parameters γ and η are obtained from Eq. (22) and translated into the evolution path in Fig. 4.

6 THE SMBH DISTRIBUTION IN γ-η PLANE

With five length scales defined in Eqs. (15), (16), and (17), we will identify the upper and lower limits of SMBH distribution and the boundary for active and inactive SMBHs.

(i) The upper limit is determined by setting the scales $r_p = r_B$. The maximum radiation scale r_p cannot exceed r_B, the sphere of BH influence. Beyond that limit, the gravity of black hole is not sufficient to balance the radiation pressure. From Eq. (20), we have

$$\gamma\eta = \frac{(3\alpha_r^2\gamma_r)^{5/4}}{\alpha_r} \approx 12 \quad \text{(Red solid line in Fig. 4).} \tag{23}$$

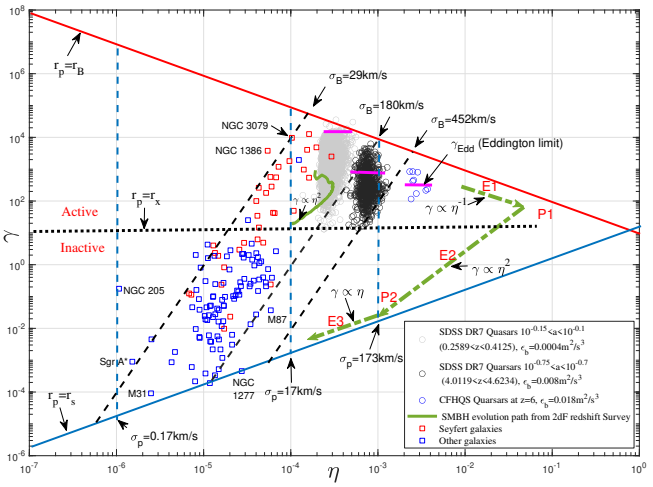

Figure 4. The distribution and evolution of SMBHs in the plane of γ-η. The distribution of SMBHs from Table A1 is presented as square symbols in red (Seyfert) and blue (other). The gray and black circles are distributions of quasars from SDSS DR7 at $z \approx 0.33$ and $z \approx 4.3$. The blue circles are high redshift quasars from CFHQS survey. Eddington limit is presented as magenta lines. The upper limit of distribution (red solid line), lower limit (blue solid line), and the boundary for active and inactive SMBHs (black dotted line) are discussed in Section 6. The evolution of a typical SMBH (green solid line) is mapped onto γ-η plane using the data from 2dF Redshift Survey. The green dash line represents the postulated evolution path of SMBH with three stages (E1, E2, and E3) and two turning points (P1 and P2) (see Section 7).

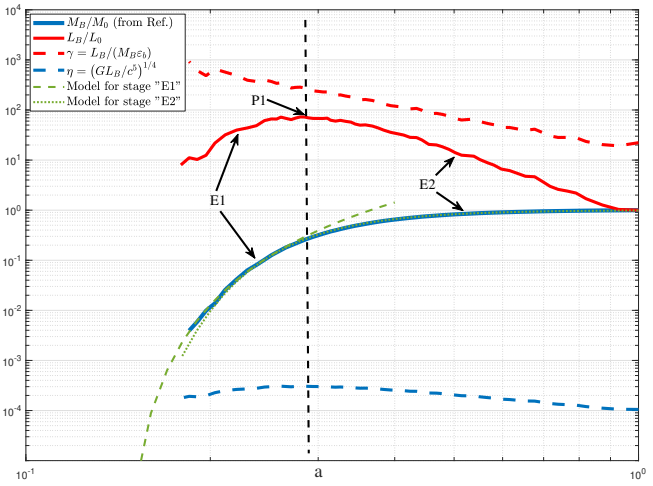

Figure 5. The variation of BH mass (M_B) and luminosity (L_B) of a typical SMBH with scale factor a. The mass evolution is obtained from quasar luminosity function from 2dF Redshift Survey (Yu & Tremaine 2002). The luminosity evolution is derived from M_B using Eq. (22) that has a maximum BH luminosity at $a \approx 0.28$. The evolution of two parameters γ and η is computed by Eq. (18) and mapped onto the γ-η plane (solid green line in Fig. 4). The proposed model of SMBH evolution in Eqs. (45) and (52) (green dash and dotted lines) is also presented for comparison with good agreement.

Substituting Eq. (18) into (23), the upper limit of BH luminosity L_B is related to physics on bulge scale through $r_p = r_B$,

$$L_B = 3\alpha_r^{6/5}\gamma_r\varepsilon_b^{4/5}M_B^{4/5}G^{-1/5}c. \tag{24}$$

(ii) The lower limit is determined by setting the scales $r_p = r_s$, i.e the minimum radiation scale r_p cannot be less than Schwarzschild

radius r_s. From Eq. (20), we should have

$$\gamma = 2(3\alpha_r^2\gamma_r)^{3/4}\eta \approx 24\eta \quad \text{(Blue solid line in Fig. 4).} \tag{25}$$

Similarly, the lower limit of BH luminosity L_B should be related to the physics on black hole scale through $r_p = r_s$,

$$L_B = 2^{4/3}(3\alpha_r^2\gamma_r)\varepsilon_b^{4/3}M_B^{4/3}G^{1/3}c^{-5/3}. \tag{26}$$

(iii) Velocity dispersion $\sigma_p^2 \propto (\varepsilon_b r_p)^{2/3}$ (Eq. (10)) on scale r_p should read (using r_p in Eq. (16))

$$\frac{\sigma_p}{c} = \left(\frac{\gamma_r}{3}\right)^{\frac{1}{4}}\eta \quad \text{or} \quad L_B = \frac{3c}{\gamma_r G}\sigma_p^4. \tag{27}$$

The luminosity $L_B \propto \sigma_p^4$ such that constant η leads to constant σ_p (the blue dash lines in Fig. 4).

Equation (27) shares a similar form as that derived from the momentum-driven outflow (King 2003; Marsden et al. 2020), while the theoretical origins seems entirely different. In Eq. (27), the radiation force due to actual BH luminosity $F_p = L_B/c$ must balance the cascade force (see F_r in Eq. (10)),

$$F_P = \frac{L_B}{c} = F_r = \frac{3}{\gamma_r}\frac{\sigma_p^4}{G}. \tag{28}$$

No gas density profile is required in this formulation.

While for momentum-driven outflow, by assuming an isothermal mass density $\rho = \sigma^2/(2\pi G r^2)$ for matter including both gas and dark matter, the mass of gas M_{gas} enclosed in radius R and the weight W_{gas} are

$$M_{gas} = 2f_g\sigma^2 R/G \quad \text{and} \quad W_{gas} = M_{gas}V_{cir}^2/R. \tag{29}$$

Here $f_g \approx 0.16$ is the cosmological gas (baryon) fraction in total matter and σ is the velocity dispersion. The circling velocity $V_{cir}^2 = GM/R = 2\sigma^2$, where M is the total mass including both dark matter and gas. The AGN wind momentum (on the order of L_{Edd}, not the actual BH luminosity L_B) balances the weight of gas W_{gas},

$$\frac{L_{Edd}}{c} = W_{gas} = \frac{4f_g\sigma^4}{G}, \tag{30}$$

such that the BH mass $M_B \propto \sigma^4$. More study should be explored for comparison between Eqs. (28) and (30). Next, we will demonstrate $M_B \propto \sigma_b^5$ from the theory of cascade (Eq. (32)).

(iv) Similarly, velocity dispersion σ_B on scale r_B simply reads (using Eq. (10) for σ_B and Eq. (15) for r_B)

$$\frac{\sigma_B}{c} = \frac{(\alpha_r\gamma_r)^{1/2}}{\alpha_r^{1/5}}\left(\frac{\eta^4}{\gamma}\right)^{\frac{1}{5}} \quad \text{or} \quad M_B = \alpha_r^{-3/2}\gamma_r^{-5/2}\frac{\sigma_B^5}{\varepsilon_b G}, \tag{31}$$

such that we should have constant σ_B along constant η^4/γ lines (the black dash lines in Fig. 4). Therefore, the BH mass $M_B \propto \sigma_B^5$ and can be further related to the velocity dispersion σ_b on bulge scale r_b as (using Eq. (21) for the ratio σ_B/σ_b),

$$M_B = \left[\alpha_r^{-3/2}\gamma_r^{-5/2}\left\langle\frac{M_B}{M_b}\right\rangle\right]\frac{\sigma_b^5}{\varepsilon_b G}. \tag{32}$$

With the average local mass ratio $\langle M_B/M_b\rangle = [0.002\ 0.003]$ (Marconi & Hunt 2003) and $\varepsilon_b = 10^{-4}m^2/s^3$, this relation matches the local M_B-σ relation in Eq. (3) (Ferrarese & Ford 2005),

$$\frac{M_B}{10^8 M_\odot} \approx \left(\frac{\sigma_b}{200km/s}\right)^5. \tag{33}$$

(v) The boundary of active and inactive SMBHs is set by scales $r_p = r_x$. From Eq. (20), we should have

$$\gamma = 6z_r\alpha_r^2\gamma_r \approx 18.6. \tag{34}$$

This critical value of γ can be roughly used to classify black holes into the active and inactive (black dotted horizontal line in Fig. 4). Most Seyfert galaxies (red square) are above that boundary, while other galaxies (blue square) are below that boundary. The distribution of quasars is also bounded between that boundary and the upper limit (red solid line in Fig. 4). An equivalent interpretation of that boundary with a constant value of γ is also briefly discussed here: the actual BH mass accretion rate $\dot{M}_B \propto L_B/c^2$, while the mass flow rate at Schwarzschild radius r_s for dissipationless flow is (from Eqs. (11) and (15)), such that

$$\dot{m}_s \propto \varepsilon_b G^{-1} r_s \propto \varepsilon_b M_B/c^2. \tag{35}$$

Therefore, active SMBHs have an accretion rate $\dot{M}_B \gg a_r\dot{m}_s$, while inactive SMBHs have an accretion rate $\dot{M}_B \ll a_r\dot{m}_s$, where a_r is a numerical constant.

7 THE SMBH EVOLUTION IN γ-η PLANE

With upper and lower limits identified, a three-stage SMBH evolution model can be established. Let's first find the general evolution of BH mass M_B for a given power-law BH luminosity L_B. Examples are shown in Eqs. (24) and (26). Let's assume a general form

$$L_B = \alpha_0\varepsilon_b^p M_B^{1-\sigma}, \tag{36}$$

where the pre-factor α_0, exponents p and σ can be different at different stages. The evolution of BH mass M_B is related to L_B:

$$\frac{dM_B}{dt} = L_B\frac{1-\epsilon}{\epsilon c^2}. \tag{37}$$

Substituting L_B in Eq. (36) and the rate of energy cascade $\varepsilon_b = \varepsilon_0 a^{-m}$ (Eq. (14)), we can convert Eq. (37) into the BH mass evolution with respect to scale factor a,

$$\frac{d(M_B/M_0)}{da} = \beta_0 a^{-mp+\frac{1}{2}}\left(\frac{M_B}{M_0}\right)^{1-\sigma}, \tag{38}$$

where M_0 is an arbitrary scale of mass. We may choose $M_0 = M_B(a=1)$. The dimensionless β_0 and the time scale t_x read

$$\beta_0 = \frac{1}{H_0 t_x} \quad \text{and} \quad t_x = \frac{\epsilon c^2}{(1-\epsilon)\alpha_0\varepsilon_0^p M_0^{-\sigma}}. \tag{39}$$

This leads to a general solution for BH mass M_B,

$$M_B = M_\infty\left[1 - \frac{\sigma}{|\sigma|}\left(\frac{a}{a_i}\right)^{-mp+\frac{3}{2}}\right]^{\frac{1}{\sigma}}, \tag{40}$$

where $M_\infty = M_B(t=\infty)$ is the limiting BH mass. The scale factor a_i can be related to constant β_0 as

$$\beta_0 = \left(\frac{M_\infty}{M_0}\right)^\sigma\frac{mp-3/2}{|\sigma|}a_i^{mp-\frac{3}{2}}. \tag{41}$$

Now we are ready to derive the SMBH evolution that can be divided into three stages:

(i) Co-evolution stage ("E1" of green dash line in Fig. 4 that is parallel to the upper limit, also shown in Fig. 5). In this stage, the

radiation scale $r_p \propto r_B$ and SMBH evolves along line $\gamma \propto \eta^{-1}$. Let's assume $r_p = \xi_r r_B$ with constant $\xi_r \leqslant 1$, the BH evolution follows

$$\gamma\eta = \frac{(3\alpha_r^2\gamma_r)^{5/4}}{\alpha_r}\xi_r^{5/3}. \tag{42}$$

Since $r_p \propto r_B$, SMBH and host galaxy evolve together with significant increase in both size and mass. In this stage, the BH luminosity L_B is on the same order of the energy injected into the bulge, i.e. $L_B \approx \varepsilon_b M_b \gg \varepsilon_b M_B$ or $\beta \approx 1$ and $\gamma \gg 1$. The energy injected into the bulge ($\varepsilon_b M_b$) is mostly dissipated by SMBH. With decreasing γ, the mass ratio $M_B/M_b = 1/\gamma$ increases significantly in this stage. Majority of SMBH and galaxy mass are obtained during this stage. The mass ratio M_B/M_b is pretty much determined at point P1 (Figs. 4 and 5) when luminosity reaches its maximum, if galaxy merger is not considered. The BH luminosity reads (Eq. (24))

$$L_B = 3\alpha_r^{6/5}\gamma_r\xi_r^{4/3}\varepsilon_b^{4/5}M_B^{4/5}G^{-1/5}c. \tag{43}$$

The Eddington ratio should read

$$\lambda_{Edd} = \frac{L_B}{L_{Edd}} \propto \frac{\varepsilon_b^{4/5}c}{\varepsilon_{Edd}M_B^{1/5}G^{1/5}} \propto a^{-2}M_B^{-1/5}, \tag{44}$$

where the Eddington rate $\varepsilon_{Edd} = L_{Edd}/M_B = 6.3m^2/s^3$ with Eddington luminosity $L_{Edd} = 1.26\times10^{38}(M_B/M_\odot)$ erg/s.

For $m = 5/2$ from Eq. (14), $p = 4/5$ and $\sigma = 1/5$ from Eq. (43), there exists a starting time $a_i = a_1$ when SMBH is formed and starting to grow. The simplified evolution of SMBH mass in this stage can be obtained from the general solution in Eq. (40),

$$M_B = M_{\infty1}\left[1 - \left(\frac{a}{a_1}\right)^{-\frac{4}{5}m+\frac{3}{2}}\right]^5, \tag{45}$$

where the BH formation time a_1 is related to β_0 via Eq. (41),

$$\beta_0 = 3\alpha_r^{6/5}\gamma_r\xi_r^{4/3}\frac{1-\epsilon}{\epsilon}\frac{\varepsilon_0^{4/5}M_0^{-1/5}G^{-1/5}}{cH_0}. \tag{46}$$

The earlier SMBH is formed (or the smaller a_1 in Eq. (45)), the faster it grows initially (see Eq. (45)). Individual SMBH might have different values of ξ_r and a_1. However, for evolution of a typical SMBH from quasar luminosity function (solid green line in Fig. 4), $\xi_r = r_p/r_B \approx 0.052$ and $M_0 = 10^9 M_\odot$, we should have $\beta_0 \approx 2.5$ and $a_1 \approx 0.142$ from Eq. (41). The accretion model (Eq. (45)) for the evolution of a typical SMBH in this stage is plotted in Fig. 5 as the green dash line that matches the BH mass evolution from quasar luminosity function (blue solid line). Here the limiting mass $M_{\infty1}/M_0 = 131.8$ gives the best fit, where $M_{\infty1}$ is the limiting mass if SMBH continues to grow according to Eq. (45) for its entire life. Since SMBH will evolve into the second stage with a much slower growth, $M_{\infty1}$ can be much larger than the true final limiting mass.

At the end of this stage (point "P1"), the BH luminosity L_B reaches its maximum (due to decreasing ε_b and increasing M_B in Eq. (43)). In this stage, we can also find the BH mass evolving as $M_B \propto \sigma_p^5$ (from Eqs. (27) and (43)),

$$M_B = \left[\alpha_r^{-3/2}\gamma_r^{-5/2}\xi_r^{-5/3}\right]\frac{\sigma_p^5}{\varepsilon_b G}. \tag{47}$$

(ii) Transitional stage ("E2" of green dash line in Fig. 4 and in Fig. 5) following the scaling $\gamma \propto \eta^2$. In this stage, the ratio r_B/r_p increases with time (see Eq. (20)) because of the decreasing luminosity L_B or η. With decreasing β and γ, the energy injected into the host galaxy ($\varepsilon_b M_b$) is only partially dissipated by SMBH. More stars are formed in the host galaxy and radiating away the energy gained by the release of gravitational potential. The BH luminosity L_B starts to decrease with a small increase in BH mass M_B and bulge mass M_b.

This stage is well between the upper and lower limits in Fig. 4, where the radiation scale $r_s \ll r_p \ll r_B$. In this range, the luminosity L_B is only dependent on the energy cascade ε_b and the BH mass M_B, and not influenced by the physics on both galaxy and black hole scale (see Eq. (43) and (26) in other two stages for comparison). Therefore, constants G and c are not involved in this stage. Without loss of generality, L_B can be expressed as functions of ε_b and M_B only. From a simple dimensional analysis, L_B reads

$$L_B = \gamma^*\varepsilon_b^p M_B(\varepsilon_b^*)^{1-p}, \tag{48}$$

where p is an exponent to be determined. Symbols γ^* and ε_b^* stand for the value of γ and ε_b at point "P1" (superscript '*' stands for that value at "P1" in Figs. 4 and 5). Equation (48) can be rewritten as

$$\frac{\gamma}{\gamma^*} = \left(\frac{\varepsilon_b}{\varepsilon_b^*}\right)^{p-1} \approx \beta = \frac{L_B}{\varepsilon_b M_b}, \tag{49}$$

where we postulate that the mass ratio $M_B/M_b = \beta/\gamma = 1/\gamma^*$ does not vary in this stage. In addition, a reasonable guess is a constant density $\rho_p \equiv \rho_r(r = r_p)$ at r_p during evolution. Otherwise, density ρ_p at r_p diverges or vanishes with time. From Eqs. (9), (16) and (48), we should have the scaling $\rho_p \propto \varepsilon_b^{2-p}$, i.e.

$$\rho_p = 3\alpha_r^2\beta_r\gamma_r\left(\frac{\varepsilon_b}{\varepsilon_b^*}\right)^{2-p}\frac{\varepsilon_b^* c}{\gamma^* M_B G^2}. \tag{50}$$

A constant ρ_p during evolution in this stage simply requires $p = 2$. Other relevant quantities on scale r_p during SMBH evolution are: velocity $\sigma_p \propto \varepsilon_b^{1/2}$, scale $r_p \propto \varepsilon_b^{1/2}$, and pressure $P_p = \rho_p\sigma_p^2 \propto \varepsilon_b$. Equivalent relation of Eq. (48) in γ-η plane is (Eqs. (18) and (20))

$$\gamma = \left[\alpha_r^{3/2}\gamma_r^{5/2}\left(\frac{\sigma_B^*}{c}\right)^{-5}\right]^{1-\frac{1}{p}}\gamma^{*\frac{1}{p}}\eta^{4-\frac{4}{p}}\left(\frac{M_B^*}{M_B}\right)^{1-\frac{1}{p}}, \tag{51}$$

where the exponent $p = 2$ can be confirmed by the evolution of SMBH in Fig. 4. For late in this stage with an almost constant M_B, $\gamma \propto \eta^2$ in this range.

With BH luminosity L_B from Eq. (48) in this stage, the solution of M_B simply reads

$$M_B = M_{\infty2}\exp\left[-\left(\frac{a}{a_2}\right)^{-mp+\frac{3}{2}}\right], \tag{52}$$

where the scale factor a_2 that determines the speed of growth reads,

$$\beta_0 = \frac{(1-\epsilon)\gamma^*\varepsilon_0^p\varepsilon_b^{*\,1-p}}{\epsilon c^2 H_0} = \left(mp - \frac{3}{2}\right)a_2{}^{mp-\frac{3}{2}}. \tag{53}$$

Individual SMBH might have different parameters γ^* and ε_b^*. For the evolution of a typical SMBH in Figs. 4 and 5, the time to reach the maximum luminosity is $a^* \approx 0.28$ with $\gamma^* \approx 250$ and $\varepsilon_b^* \approx 0.0025m^2/s^3$, such that $a_2 \approx 0.31$. With $M_{\infty2} = M_0 = 10^9 M_\odot$, the proposed accretion model in this stage (Eq. (52)) is also presented in Fig. 5 that is in very good agreement with the BH mass accretion from quasar luminosity function. The SMBH in this stage is initially active and becomes inactive when γ is less than the critical value of γ in Eq. (34). The evolution of a typical SMBH stops at that critical value, i.e. the end of quasar phase (green solid line in Fig. 4).

Table 1. Physical quantities for three stages of SMBH evolution (values of M_∞ and a_i are for the evolution of a typical SMBH in Figs. 4 and 5).

Quantity	Stage "E1"	Stage "E2"	Stage "E3"
L_B	Eq. (43)	Eq. (48)	Eq. (26)
M_B	Eq. (45)	Eq. (52)	Eq. (55)
m	5/2	5/2	5/2
p	4/5	2	4/3
σ	1/5	0	-1/3
M_∞	$131.8M_0$	M_0	M_0
a_i	0.142	0.31	1.8×10^{-4}

Finally, in this stage, the BH mass M_B evolves as $M_B \propto \sigma_p^4$ (from Eqs. (27) and (48)),

$$M_B = \left(\frac{3}{\gamma_r\gamma^*}\right)\left(\frac{\varepsilon_b}{\varepsilon_b^*}\right)^{1-p}\frac{\sigma_p^4 c}{\varepsilon_b G}. \tag{54}$$

(iii) Dormant stage with $\gamma \propto \eta$ ("E3" of green dash line in Fig. 4). In this stage, the radiation scale equals the Schwarzschild radius, i.e. $r_p = r_s$ that leads to the lower limit in Fig. 4. Substituting L_B in Eq. (26) and $\varepsilon_b = \varepsilon_0 a^{-m}$ in Eq. (10), solution of M_B can be obtained from the general solution (Eq. (40)) with $m = 5/2$, $p = 4/3$, and $\sigma = -1/3$,

$$M_B = M_{\infty 3}\left[1+\left(\frac{a}{a_3}\right)^{-\frac{4}{3}m+\frac{3}{2}}\right]^{-3}, \tag{55}$$

with corresponding β_0

$$\beta_0 = 2^{\frac{4}{3}}\left(3\alpha_r^2\gamma_r\right)\frac{1-\epsilon}{\epsilon}\frac{\varepsilon_0^{4/3}M_0^{1/3}G^{1/3}}{c^{11/3}H_0}. \tag{56}$$

With $M_{\infty 3} = M_0 = 10^9 M_\odot$, $\beta_0 \approx 8\times10^{-7}$, we should have $a_3 \approx 1.8\times10^{-4}$ from Eq. (41). For such a small a_3, BH mass M_B should be almost a constant in this stage. In addition, the BH mass M_B evolves as $M_B \propto \sigma_p^3$ in this stage (from Eqs. (26) and (27)),

$$M_B = \left(\frac{\alpha_r^{-3/2}\gamma_r^{-3/2}}{2}\right)\frac{\sigma_p^3 c^2}{\varepsilon_b G}. \tag{57}$$

8 BEYOND THE EDDINGTON LIMIT

In this section, we demonstrate that it is possible the proposed accretion model in Eq. (45) (first stage of SMBH evolution) exceeds the Eddington limit. For the standard Eddington limit, the pressure due to BH luminosity at a distance r is balanced by BH gravity, i.e.

$$\frac{L_{Edd}}{4\pi c r^2} = \frac{GM_B m_p}{r^2\sigma_T} \quad \text{or} \quad \frac{L_{Edd}}{c} \approx M_B \times \left(2.1\times10^{-8}\frac{m}{s^2}\right), \tag{58}$$

where $\sigma_T \approx 6.65\times10^{-29}m^2$ is the Thomson scattering cross-section for electron and $m_p \approx 1.67\times10^{-27}kg$ is the mass of a proton. The Eddington limit is formulated for static gas surrounding a BH.

The Eddington limit corresponding to a Eddington value of γ, i.e. $\gamma_{Edd} = L_{Edd}/(\varepsilon_b M_B) = \varepsilon_{Edd}/\varepsilon_b$, where the Eddington rate $\varepsilon_{Edd} = L_{Edd}/M_B = 6.3m^2/s^3$. The Eddington γ, i.e. γ_{Edd}, is plotted in Fig. 4 as solid magenta lines for quasars from SDSS DR7 and CFHQS survey. Obviously, some quasars can have a luminosity exceeding the Eddington limit in the early universe.

In our accretion model, gas is never a static medium surrounding a SMBH. Instead, gas forms a turbulent medium involving energy cascade with a rate of ε_b that is scale independent, i.e. the same rate from bulge scale r_b down to the radiation scale r_p. Since $\varepsilon_b \propto a^{-5/2}$, the Eddington $\gamma_{Edd} \propto a^{5/2}$ increases with time, while the value of γ always decreases with time during SMBH evolution (see Figs. 4 and 5). Hence, SMBH can evolve with a rate beyond the Eddington limit during its early stage where $\gamma > \gamma_{Edd}$.

Similarly, by combining Eqs. (27) and (47), in the first stage of this model, the radiation force from BH luminosity must balance the force from energy cascade (or turbulence kinetic pressures),

$$\frac{L_B}{c} \propto \frac{\sigma_p^4}{G} \propto M_B \times \left(\frac{\varepsilon_b}{\sigma_p}\right). \tag{59}$$

Since ε_b decreases with time and σ_p increases with time (due to increasing L_B in Eq. (27)), compared with Eq. (58), there exists a period $L_B > L_{Edd}$ in the first stage of evolution. At that time, the radiation pressure must support a cascade pressure that is greater than the pressure from the static weight of surrounding gas. Therefore, the BH luminosity is possible to exceed the Eddington limit due to large values of ε_b in the early universe.

To better illustrate this, Figure 6 presents the comparison between the Eddington accretion and our accretion model based on the co-evolution of SMBH and host galaxy (Eqs. (45) and (52)). For Eddington accretion, BH mass follows an exponential growth as,

$$M_B = M_i \exp\left(\frac{t-t_i}{t_{sal}}\right), \tag{60}$$

where M_i is the seed BH mass at an earlier epoch z_i, t and t_i are the current age and the cosmic age at z_i. The time scale $t_{sal} = 4.5\times10^8\epsilon/(1-\epsilon)$ yrs is the Salpeter time or e-folding time, where radiative efficiency $\epsilon = 0.1$. Figure 6 plots the Eddington accretion with seed BH mass $M_i = 10M_\odot$ and $M_i = 100M_\odot$ at $z_i = 20$ (green lines) and at $z_i = 30$ (blue lines). This is selected from the reasonable range of seed BH mass from a Pop III star remnant at $z \approx 20-30$. For that range of seed BH mass, it is challenging for Eddington accretion to produce the accreting SMBH with a mass of $10^9 M_\odot$ observed out to redshifts $z > 6$ (green circle).

The proposed accretion model (Eq. (45)) in the first stage (E1) of evolution does not require an initial seed BH mass M_i. It only requires an initial time a_i when SMBH was formed and the limiting mass $M_{\infty 1}$ if BH keeps growing according to this model. The value of $M_{\infty 1}$ can be much larger than the actual BH limiting maximum mass M_0 because BH grows much slower in the second and third stages. Figure 6 plots the proposed accretion model with with $M_{\infty 1} = 2.2\times10^{11}M_\odot$ and $M_{\infty 2} = 2\times10^9 M_\odot$ at $z_i = 20$ and $z_i = 30$ (red lines for stage E1 and black lines for stage E2). It is possible that SMBH can have a mass exceeding the Eddington limit at its early stage and reach a BH mass of $10^9 M_\odot$ at redshift $z = 7$.

Finally, the parameter $M_{\infty 1}$ can be determined from the continuity condition between the first and second stages. The time of transition (a^*) between two stages is the time of maximum luminosity L_B. By taking derivative of L_B in Eq. (48) with M_B from Eq. (52), we have

$$\left(\frac{a^*}{a_2}\right)^{-mp+\frac{3}{2}} = \frac{2m}{mp-3/2}. \tag{61}$$

With $m = 5/2$ and $p = 2$, the ratio $a^*/a_2 \approx 0.9$, i.e. $a_2 \approx a^*$ is approximately the transition time. By setting the BH mass of the first

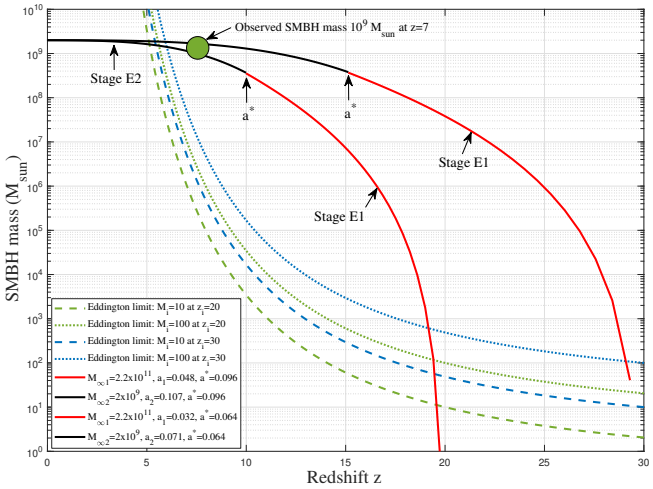

Figure 6. The variation of SMBH mass M_B with redshift z for i) a simple continuous Eddington accretion (Eq. (60)); The green/blue dash/dotted lines are Eddington-limited growth models from a seed BH with mass $M_i = 10M_\odot$ and $M_i = 100M_\odot$ at $z_i = 20$ and $z_i = 30$; ii) the proposed accretion model in Eqs. (45) and (52) for SMBH formed at the same z_i with limiting BH mass $M_{\infty 1} = 2.2 \times 10^{11} M_\odot$ and $M_{\infty 2} = 2 \times 10^9 M_\odot$ (red and black lines). Initial seed BH mass is not required is this model.

stage (Eq. (45)) should equal the mass of the second stage (Eq. (52)) at transition time a^*, we have the mass ratio

$$\frac{M_{\infty 1}}{M_{\infty 2}} = \left[1 - \left(\frac{a^*}{a_1}\right)^{-\frac{4}{5}m+\frac{3}{2}}\right]^{-5} \exp\left[-\left(\frac{a^*}{a_2}\right)^{-mp+\frac{3}{2}}\right] = 0.24\left[1 - \left(a^*/a_1\right)^{-\frac{1}{2}}\right]^{-5}, \quad (62)$$

where Eq. (61) is substituted. $M_{\infty 2} = M_0$ is the BH limiting mass at $a = 1$. Therefore, parameter $M_{\infty 1}$ is determined by the ratio a^*/a_1, i.e. the ratio of transition time and the time SMBH is formed. For a typical SMBH from quasar luminosity function (in Figs. 4 and 5), $a^*/a_1 \approx 2$ such that $M_{\infty 1}/M_{\infty 2} \approx 110$ for Fig. 6.

9 CONCLUSION

The constant rate of energy cascade ε_u can be identified in the self-gravitating collisionless dark matter flow from the energy evolution and galaxy rotation curves. Energy cascade also exists in the dynamics of bulge with a scale-independent, but time varying rate of cascade $\varepsilon_b \propto a^{-5/2}$. The bulge mass-size relation can be expressed as $M_b \propto \varepsilon_b^{2/3} r_b^{5/3}$ or bulge density-size relation as $\rho_b \propto \varepsilon_b^{2/3} r_b^{-4/3}$, as confirmed by galaxy data. We demonstrate the energy cascade from galaxy bulge down to the black hole scale can regulate the co-evolution of SMBHs and their host galaxies. Five relevant length scales are defined according to the dominant physics on that scale, i.e. the bulge scale r_b, the BH sphere of influence r_B, the radiation scale r_p, the dissipation scale r_x, and the Schwarzschild radius r_s. By introducing two dimensionless parameters $\gamma = L_B/(M_B\varepsilon_b)$ and $\eta = (GL_B/c^5)^{1/4}$, the distribution and evolution of SMBHs can be mapped onto the γ-η plane. Upper and lower limits, and the active/inactive boundary are identified for the distribution of SMBHs by setting scales $r_p = r_B$, $r_p = r_s$, and $r_p = r_x$. Similarly, a three-stage evolution model (co-evolution, transition, and dormant) is proposed for the evolution of SMBH that follows $\gamma \propto \eta^{-1}$, $\gamma \propto \eta^2$ and $\gamma \propto \eta$, respectively. Since ε_b is much larger in the early universe, the SMBH accretion can exceed the Eddington limit during its early stage, where the radiation force or pressure from BH luminosity must balance the cascade force or pressure due to the energy cascade that is greater than the weight of static surrounding gas.

DATA AVAILABILITY

Dataset for this article is available on Zenodo (Xu 2022a), along with the accompanying presentation "A comparative study of dark matter flow & hydrodynamic turbulence and its applications".

REFERENCES

Babyk I. V., McNamara B. R., Nulsen P. E. J., Hogan M. T., Vantyghem A. N., Russell H. R., Pulido F. A., Edge A. C., 2018, The Astrophysical Journal, 857, 32

Beifiori A., Sarzi M., Corsini E. M., Dalla Bonta E., Pizzella A., Coccato L., Bertola F., 2009, Astrophysical Journal, 692, 856

Beifiori A., Courteau S., Corsini E. M., Zhu Y., 2012, Monthly Notices of the Royal Astronomical Society, 419, 2497

Bender R., Kormendy J., Cornell M. E., Fisher D. B., 2015, Astrophysical Journal, 807

Benedetto E., Fallarino M. T., Feoli A., 2013, Astronomy & Astrophysics, 558

Bennert N., Jungwiert B., Komossa S., Haas M., Chini R., 2006, Astronomy & Astrophysics, 446, 919

Bettoni D., Falomo R., Fasano G., Govoni F., 2003, Astronomy & Astrophysics, 399, 869

Bogdan A., Lovisari L., Volonteri M., Dubois Y., 2018, Astrophysical Journal, 852

Boizelle B. D., et al., 2021, Astrophysical Journal, 908

Brightman M., et al., 2017, Astrophysical Journal, 844

Burtscher L., et al., 2015, Astronomy & Astrophysics, 578

Cappellari M., et al., 2011, Monthly Notices of the Royal Astronomical Society, 413, 813

Cappellari M., et al., 2013, Mon. Not. Roy. Astron. Soc., 432, 1862

Castangia P., Panessa F., Henkel C., Kadler M., Tarchi A., 2013, Monthly Notices of the Royal Astronomical Society, 436, 3388

Chae K. H., Bernardi M., Sheth R. K., 2018, Astrophysical Journal, 860

Coccato L., Sarzi M., Pizzella A., Corsini E. M., Dalla Bonta E., Bertola F., 2006, Monthly Notices of the Royal Astronomical Society, 366, 1050

Das M., Teuben P. J., Vogel S. N., Regan M. W., Sheth K., Harris A. I., Jefferys W. H., 2003, Astrophysical Journal, 582, 190

Davis B. L., Graham A. W., Cameron E., 2019, Astrophysical Journal, 873

Ding X., Treu T., Silverman J. D., Bhowmick A. K., Menci N., Di Matteo T., 2020, ApJ, 896, 159

Dullo B. T., Martinez-Lombilla C., Knapen J. H., 2016, Monthly Notices of the Royal Astronomical Society, 462, 3800

Fabian A. C., Sanders J. S., Haehnelt M., Rees M. J., Miller J. M., 2013, Monthly Notices of the Royal Astronomical Society, 431, L38

Ferrarese L., Ford H., 2005, Space Sci. Rev., 116, 523

Ferrarese L., Merritt D., 2000, ApJ, 539, L9

Fisher D. B., Drory N., 2010, Astrophysical Journal, 716, 942

Frenk C. S., et al., 2000, arXiv:astro-ph/0007362v1

Gao F., et al., 2017, Astrophysical Journal, 834

Garcia-Bernete I., et al., 2021, Astronomy & Astrophysics, 645

Gonzalez-Martin O., Masegosa J., Marquez I., Guainazzi M., Jimenez-Bailon E., 2009, Astronomy & Astrophysics, 506, 1107

Graham A. W., Scott N., 2013, ApJ, 764, 151

Gultekin K., et al., 2009a, Astrophysical Journal, 698, 198

Gultekin K., Cackett E. M., Miller J. M., Di Matteo T., Markoff S., Richstone D. O., 2009b, Astrophysical Journal, 706, 404

Gultekin K., Richstone D. O., Gebhardt K., Faber S. M., Lauer T. R., Bender R., Kormendy J., Pinkney J., 2011, Astrophysical Journal, 741

Gultekin K., Cackett E. M., Miller J. M., Di Matteo T., Markoff S., Richstone D. O., 2012, Astrophysical Journal, 749
Gultekin K., King A. L., Cackett E. M., Nyland K., Miller J. M., Di Matteo T., Markoff S., Rupen M. P., 2019, Astrophysical Journal, 871
Haring N., Rix H. W., 2004, Astrophysical Journal, 604, L89
Ho L. C., 2009, Astrophysical Journal, 699, 626
Ho L. C., Greene J. E., Filippenko A. V., Sargent W. L. W., 2009, Astrophysical Journal Supplement Series, 183, 1
Hopkins P. F., Hernquist L., Cox T. J., Robertson B., Krause E., 2007, ApJ, 669, 67
Hu J., 2008, Monthly Notices of the Royal Astronomical Society, 386, 2242
Huertas-Company M., et al., 2013, Monthly Notices of the Royal Astronomical Society, 428, 1715
Inayoshi K., Ichikawa K., Ho L. C., 2020, Astrophysical Journal, 894
Irvine W. M., 1961, Thesis, HARVARD UNIVERSITY
Kammoun E. S., et al., 2020, Astrophysical Journal, 901
King A., 2003, ApJ, 596, L27
Kolmogorov A. N., 1941, Comptes Rendus De L Academie Des Sciences De L Urss, 32, 16
Kormendy J., Ho L. C., 2013, Annual Review of Astronomy and Astrophysics, 51, 511
Koss M. J., et al., 2015, Astrophysical Journal, 807
Kuo C. Y., et al., 2020, Monthly Notices of the Royal Astronomical Society, 498, 1609
Lakhchaura K., Truong N., Werner N., 2019, Monthly Notices of the Royal Astronomical Society, 488, L134
Layzer D., 1963, Astrophysical Journal, 138, 174
Lelli F., McGaugh S. S., Schombert J. M., 2016, AJ, 152, 157
Li P., Lelli F., McGaugh S., Schombert J., 2020, ApJS, 247, 31
Maccarone T. J., Kundu A., Zepf S. E., Rhode K. L., 2011, Monthly Notices of the Royal Astronomical Society, 410, 1655
Machacek M. E., Jones C., Forman W. R., 2004, Astrophysical Journal, 610, 183
Magorrian J., et al., 1998, AJ, 115, 2285
Marconi A., Hunt L. K., 2003, Astrophysical Journal, 589, L21
Marconi A., et al., 2003, Astrophysical Journal, 586, 868
Marin F., 2016, Monthly Notices of the Royal Astronomical Society, 460, 3679
Marsden C., Shankar F., Ginolfi M., Zubovas K., 2020, Frontiers in Physics, 8
Martinsson T. P. K., Verheijen M. A. W., Westfall K. B., Bershady M. A., Andersen D. R., Swaters R. A., 2013, A&A, 557, A131
McConnachie A. W., 2012, Astronomical Journal, 144
McConnell N. J., Ma C. P., 2013, Astrophysical Journal, 764
McConnell N. J., Ma C. P., Graham J. R., Gebhardt K., Lauer T. R., Wright S. A., Richstone D. O., 2011, Astrophysical Journal, 728
McConnell N. J., Ma C. P., Murphy J. D., Gebhardt K., Lauer T. R., Graham J. R., Wright S. A., Richstone D. O., 2012, Astrophysical Journal, 756
Menci N., Fiore F., Bongiorno A., Lamastra A., 2016, A&A, 594, A99
Merritt D., Ferrarese L., 2001, Monthly Notices of the Royal Astronomical Society, 320, L30
Mowla L., van der Wel A., van Dokkum P., Miller T. B., 2019a, Astrophysical Journal Letters, 872
Mowla L. A., et al., 2019b, Astrophysical Journal, 880
Nagar N. M., Falcke H., Wilson A. S., 2005, Astronomy & Astrophysics, 435, 521
Parker E. N., 1958, Reviews of Modern Physics, 30, 955
Peng C. Y., 2007, ApJ, 671, 1098
Perez S., Casassus S., Cortes J. R., Kenney J. D. P., 2009, Monthly Notices of the Royal Astronomical Society, 400, 2098
Richardson L. F., 1922, Weather Prediction by Numerical Process. Cambridge University Press, Cambridge, UK
Rusli S. P., Thomas J., Erwin P., Saglia R. P., Nowak N., Bender R., 2011, Monthly Notices of the Royal Astronomical Society, 410, 1223
Rusli S. P., et al., 2013, Astronomical Journal, 146
Sahu N., Graham A. W., Davis B. L., 2019, Astrophysical Journal, 887
Samir R. M., Reda F. M., Shaker A. A., Osman A. M. I., Amin M. Y., 2016, NRIAG Journal of Astronomy and Geophysics, 5, 277
Sanchez-Portal M., Diaz A. I., Terlevich E., Terlevich R., 2004, Monthly Notices of the Royal Astronomical Society, 350, 1087
Sarzi M., et al., 2002, Astrophysical Journal, 567, 237
Schneider D. P., et al., 2010, The Astronomical Journal, 139, 2360
Shen S. Y., Mo H. J., White S. D. M., Blanton M. R., Kauffmann G., Voges W., Brinkmann J., Csabai I., 2003, Monthly Notices of the Royal Astronomical Society, 343, 978
Shen Y., et al., 2011, ApJS, 194, 45
Silk J., Rees M. J., 1998, A&A, 331, L1
Sofue Y., 2016, Publications of the Astronomical Society of Japan, 68
Spolaor M., Forbes D. A., Hau G. K. T., Proctor R. N., Brough S., 2008, Monthly Notices of the Royal Astronomical Society, 385, 667
Swartz D. A., Yukita M., Tennant A. F., Soria R., Ghosh K. K., 2006, Astrophysical Journal, 647, 1030
Urquhart R., McDermott L. I., Strader J., Seth A. C., Chomiuk L., Neumayer N., Nguyen D. D., Tremou E., 2022, The Astrophysical Journal, 940, 111
Weinzirl T., Jogee S., Khochfar S., Burkert A., Kormendy J., 2009, Astrophysical Journal, 696, 411
White S. D. M., Rees M. J., 1978, MNRAS, 183, 341
Williams D. R. A., et al., 2022, Monthly Notices of the Royal Astronomical Society, 510, 4909
Willott C. J., et al., 2010, The Astronomical Journal, 140, 546
Woo J.-H., Yoon Y., Park S., Park D., Kim S. C., 2015, The Astrophysical Journal, 801, 38
Wrobel J. M., Terashima Y., Ho L. C., 2008, Astrophysical Journal, 675, 1041
Xu Z., 2022a, A comparative study of dark matter flow & hydrodynamic turbulence and its applications, doi:10.5281/zenodo.6569901, http://dx.doi.org/10.5281/zenodo.6569901
Xu Z., 2022b, arXiv e-prints, p. arXiv.2209.03313
Yang L., Roberts-Borsani G., Treu T., Birrer S., Morishita T., Bradac M., 2020, Monthly Notices of the Royal Astronomical Society, 501, 1028
Yu Q. J., Tremaine S., 2002, Monthly Notices of the Royal Astronomical Society, 335, 965
Zhang W. M., Soria R., Zhang S. N., Swartz D. A., Liu J. F., 2009, Astrophysical Journal, 699, 281
van den Bosch R. C. E., Gebhardt K., Gueltekin K., van de Ven G., van der Wel A., Walsh J. L., 2012, Nature, 491, 729

APPENDIX A: SMBH AND HOST GALAXY DATA

Table A1. Samples of SMBHs and their host galaxies

Galaxy Name	Type	M_B ($M_\odot$)	Ref.	L_B (erg/s)	Ref.	σ_b (km/s)	Ref.	σ_B (km/s)	σ_p (km/s)	M_b ($M_\odot$)	Ref.	r_b (kpc)	r_B (kpc)	r_p (kpc)	r_x (kpc)	r_s (kpc)	ε_b (m^2/s^3)
Cygnus A	Seyfert	2.7E+09	5	2.7E+45	2	270.0	1	67.1	38.2	1.6E+12	1	31.6	4.8E-01	9.0E-02	3.1E-03	2.6E-07	2.0E-05
A1836-BCG		3.9E+09	1	3.3E+42	5	288.0	1	89.6	7.2	7.6E+11	1	13.2	4.0E-01	2.0E-04	3.1E-03	3.7E-07	5.9E-05
Circinus	Seyfert	1.1E+06	5	4.8E+42	2	158.0	1	29.2	7.9	3.0E+09	1	0.2	1.1E-03	2.1E-05	3.7E-06	1.1E-10	7.4E-04
IC 1262				3.6E+43	63	232.5	63		13.0	9.3E+11	63	24.7		4.4E-03			1.6E-05
IC 1459		2.5E+09	5	1.3E+42	3a	340.0	1	99.4	5.6	6.6E+11	1	8.2	2.1E-01	3.8E-05	1.8E-03	2.4E-07	1.5E-04
IC 1633				8.3E+42	63	356.6	63		9.0	2.4E+12	63	27.0		4.4E-04			5.4E-05
IC 2560	Seyfert	5.0E+06	5	1.2E+42	5	137.0	1	22.7	5.6	2.3E+10	1	1.8	8.0E-03	1.2E-04	2.3E-05	4.8E-10	4.7E-05
IC 4296		1.3E+09	5	1.6E+42	3a	322.0	1	69.3	6.0	1.6E+12	1	22.2	2.2E-01	1.4E-04	1.4E-03	1.2E-07	4.9E-05
IC 5267				6.2E+40	63	167.7	63		2.6	1.5E+11	63	7.6		3.0E-05			2.0E-05
IC 5358				1.1E+44	63	214.2	63		17.2	1.6E+12	63	50.2		2.6E-02			6.3E-06
Sgr A*		4.1E+06	1	1.9E+36	3a	105.0	1	19.3	0.2	1.1E+10	1	1.4	9.0E-03	9.6E-09	2.2E-05	3.9E-10	2.6E-05
NGC193		2.5E+08	59	1.6E+41	59	187.0	59	70.5	3.4	1.9E+10	59	0.8	4.1E-02	4.4E-06	2.7E-04	2.4E-08	2.7E-04
NGC 205		3.8E+04	5	4.8E+35	58	35.0	13	5.1	0.1	3.3E+08	13	0.4	1.2E-03	2.5E-08	1.1E-06	3.7E-12	3.6E-06
NGC 221		2.5E+06	5	1.5E+37	3a	75.0	1	21.0	0.3	8.0E+08	1	0.2	4.5E-03	1.7E-08	1.2E-05	2.4E-10	6.7E-05
NGC 224		1.4E+08	5	1.4E+37	3a	160.0	1	45.4	0.3	4.4E+10	1	2.5	5.7E-02	2.1E-08	2.7E-04	1.4E-08	5.4E-05
NGC 315	BCG	1.7E+09	3	7.6E+42	3a	341.0	11	81.6	8.8	1.2E+12	11	14.9	2.0E-01	2.6E-04	1.5E-03	1.6E-07	8.6E-05
NGC 326				1.3E+42	63	231.9	63		5.7	1.4E+12	63	38.3		5.6E-04			1.1E-05
NGC 383		5.8E+08	59	9.5E+41	59	240.0	59	55.4	5.2	5.0E+11	59	12.5	1.5E-01	1.3E-04	8.5E-04	5.5E-08	3.6E-05
NGC 499				8.9E+42	63	253.3	63		9.2	5.1E+11	63	11.5		5.4E-04			4.6E-05
NGC 507	BCG	1.6E+09	3	7.3E+41	3a	331.0	12	78.1	4.9	1.3E+12	12	16.6	2.2E-01	5.4E-05	1.6E-03	1.6E-07	7.1E-05
NGC 524		8.7E+08	5	1.8E+40	5	235.0	1	67.1	1.9	2.6E+11	1	6.8	1.6E-01	3.8E-06	1.0E-03	8.3E-08	6.2E-05
NGC 533				1.3E+43	63	271.2	63		10.1	1.1E+12	63	22.4		1.2E-03			2.9E-05
NGC 541		3.9E+08	59	4.3E+41	59	191.0	59	48.5	4.3	2.1E+11	59	8.3	1.4E-01	9.4E-05	6.8E-04	3.7E-08	2.7E-05
NGC 708				3.0E+43	63	222.2	63		12.5	7.6E+11	63	22.0		3.9E-03			1.6E-05
NGC 720				6.5E+41	63	235.6	63		4.8	2.5E+11	63	6.4		5.3E-05			6.6E-05
NGC 741				5.2E+42	63	286.0	63		8.0	1.0E+12	63	17.6		3.9E-04			4.3E-05
NGC 821		1.7E+08	5	4.4E+39	2	209.0	1	49.2	1.4	1.3E+11	1	4.3	5.6E-02	1.2E-06	2.8E-04	1.6E-08	6.9E-05
NGC 1023		4.1E+07	5	1.0E+40	2	205.0	1	41.5	1.7	6.9E+10	1	2.4	2.0E-02	1.3E-06	8.7E-05	4.0E-09	1.2E-04
NGC 1052	BCG	1.7E+08	59	3.5E+40	59	191.0	59	53.8	2.3	5.6E+10	59	2.2	4.9E-02	3.8E-06	2.7E-04	1.7E-08	1.0E-04
NGC 1068	Seyfert	8.4E+06	5	2.5E+44	19a	151.0	1	30.2	21.2	1.5E+10	1	0.9	7.6E-03	2.6E-03	2.6E-05	8.1E-10	1.2E-04
NGC 1194	Seyfert	7.1E+07	5	5.5E+44	19a	148.0	1	42.8	25.7	2.0E+10	1	1.3	3.2E-02	6.9E-03	1.4E-04	6.8E-09	8.0E-05
NGC 1266				1.1E+41	63	94.4	63		3.0	1.6E+10	63	2.6		8.6E-05			1.1E-05
NGC 1277		1.7E+10	5	2.1E+41	55	403.0	14	224.5	3.6	1.8E+11	14	1.6	2.8E-01	1.1E-06	4.4E-03	1.6E-06	1.3E-03
NGC 1300		7.6E+07	5	8.2E+40	6	218.0	1	63.2	2.8	2.1E+10	1	0.6	1.5E-02	1.4E-06	9.4E-05	7.3E-09	5.3E-04
NGC 1320	Seyfert	6.0E+06	21	1.4E+44	19a	250.0	21	45.2	18.4	1.8E+10	21	0.4	2.4E-03	1.6E-04	1.1E-05	5.8E-10	1.2E-03
NGC 1316		1.7E+08	5	1.8E+40	3a	226.0	1	57.1	1.9	9.3E+10	1	2.6	4.2E-02	1.7E-06	2.4E-04	1.6E-08	1.4E-04
NGC 1332	BCG	1.5E+09	5	1.2E+40	3a	327.7	15	135.7	1.8	6.9E+10	15	0.9	6.5E-02	1.4E-07	7.1E-04	1.4E-07	1.2E-03
NGC 1374		5.9E+08	59	6.3E+39	59	167.0	59	66.7	1.5	3.3E+10	59	1.7	1.1E-01	1.2E-06	6.9E-04	5.7E-08	8.9E-05
NGC 1386	Seyfert	1.2E+06	19	3.2E+42	19a	95.0	22	16.0	7.1	5.0E+09	22	0.8	3.8E-03	3.3E-04	8.3E-06	1.2E-10	3.5E-05
NGC 1399	BCG	5.0E+08	5	9.4E+39	3a	337.0	1	88.4	1.7	2.3E+11	1	2.9	5.3E-02	3.5E-07	4.1E-04	4.8E-08	4.2E-04
NGC 1400		4.7E+09	5	7.4E+40	3a	279.0	16	124.9	2.8	1.5E+11	16	2.7	2.4E-01	2.7E-06	2.5E-03	4.5E-07	2.6E-04
NGC 1404				4.2E+42	63	228.1	63		7.6	3.3E+11	63	9.0		3.4E-04			4.3E-05
NGC 1407	BCG	4.7E+09	5	7.4E+40	3a	305.0	16	108.2	2.8	4.7E+11	16	7.3	3.3E-01	5.5E-06	3.0E-03	4.5E-07	1.3E-04
NGC 1482				3.3E+41	63	108.5	63		4.0	1.1E+11	63	13.8		7.0E-04			3.0E-06
NGC 1550	BCG	3.9E+09	5	4.5E+39	5	270.0	17	108.1	1.4	2.1E+11	17	4.2	2.7E-01	5.6E-07	2.5E-03	3.7E-07	1.5E-04
NGC 1600				2.7E+42	63	331.4	63		6.8	1.5E+12	63	19.4		1.7E-04			6.1E-05
NGC 1700				1.2E+42	63	233.1	63		5.6	3.4E+11	63	9.0		1.3E-04			4.6E-05
NGC 2273	Seyfert	7.5E+06	19	2.0E+44	19	170.0	21	36.3	20.1	9.5E+09	21	0.5	4.7E-03	7.8E-04	1.9E-05	7.2E-10	3.3E-04
NGC 2434				1.2E+41	63	183.7	63		3.2	1.2E+11	63	5.0		2.5E-05			4.0E-05
NGC 2549		1.5E+07	5	4.3E+40	51	145.0	1	31.2	2.4	1.8E+10	1	1.2	1.2E-02	5.7E-06	4.4E-05	1.4E-09	8.0E-05
NGC 2748		4.4E+07	5	1.1E+39	6	115.0	1	31.3	1.0	1.7E+10	1	1.9	3.7E-02	1.1E-06	1.3E-04	4.3E-09	2.7E-05
NGC 2768				1.2E+41	63	184.2	63		3.1	1.5E+11	63	6.2		3.0E-05			3.3E-05
NGC 2778		1.5E+07	5	2.2E+38	6	175.0	1	41.5	0.6	1.1E+10	1	0.5	6.9E-03	2.6E-08	3.1E-05	1.4E-09	3.4E-04
NGC 2787	LINER	4.1E+07	5	7.9E+39	2	189.0	1	45.4	1.6	2.9E+10	1	1.2	1.6E-02	6.9E-07	7.7E-05	3.9E-09	1.9E-04
NGC 2892		2.7E+08	59	1.1E+42	59	295.0	59	60.8	5.5	4.1E+11	59	6.8	6.0E-02	4.4E-05	3.5E-04	2.6E-08	1.2E-04
NGC 2960	Sayfert	1.1E+07	5	3.2E+40	52a	166.0	1	34.4	2.2	1.6E+10	1	0.8	7.5E-03	2.1E-06	2.9E-05	1.0E-09	1.8E-04
NGC 2974	Seyfert	1.7E+08	7	2.0E+42	48	233.0	1	55.2	6.3	1.3E+11	1	3.5	4.6E-02	6.9E-05	2.5E-04	1.6E-08	1.2E-04
NGC 3031	Seyfert	6.5E+07	5	1.1E+42	2	143.0	1	46.6	5.4	1.0E+10	1	0.7	2.4E-02	3.9E-05	1.2E-04	6.2E-09	1.3E-04
NGC 3079	Seyfert	2.4E+06	19	4.1E+43	19a	146.0	1	22.1	13.4	1.7E+10	1	1.1	4.0E-03	8.9E-04	1.1E-05	2.3E-10	8.8E-05
NGC 3091	BCG	3.7E+09	5	2.6E+42	59	297.0	17	103.7	6.8	4.1E+11	17	6.7	2.8E-01	7.8E-05	2.5E-03	3.6E-07	1.3E-04
NGC 3115		9.0E+08	5	8.2E+39	3a	230.0	1	77.2	1.6	1.2E+11	1	3.3	1.2E-01	1.1E-06	8.7E-04	8.6E-08	1.2E-04
NGC 3227	Seyfert	2.1E+07	5	5.6E+42	2	133.0	1	44.0	8.2	3.0E+09	1	0.2	8.9E-03	5.7E-05	4.1E-05	2.0E-09	3.1E-04
NGC 3245		2.4E+08	5	3.0E+40	2	205.0	1	59.1	2.2	6.8E+10	1	2.3	5.6E-02	2.9E-06	3.2E-04	2.3E-08	1.2E-04
NGC 3310		4.2E+07	5	2.1E+41	5	84.0	46	41.6	3.6	8.0E+08	45	0.2	2.0E-02	1.3E-05	8.8E-05	4.0E-09	1.2E-04
NGC 3351		8.6E+06	5	5.5E+39	57	57.0	18	17.5	1.4	1.8E+09	18	0.8	2.3E-02	1.3E-05	5.4E-05	8.3E-10	7.5E-06
NGC 3368		7.7E+06	5	1.2E+38	5	193.0	21	44.8	0.6	6.5E+09	21	0.2	3.1E-03	6.1E-09	1.5E-05	7.4E-10	9.3E-04
NGC 3377		1.8E+08	5	1.6E+39	2	145.0	1	46.1	1.1	3.1E+10	1	2.1	6.8E-02	8.3E-07	3.3E-04	1.7E-08	4.6E-05
NGC 3379	LINER	1.8E+08	5	2.3E+39	2	206.0	1	56.0	1.2	6.8E+10	1	2.3	4.6E-02	4.2E-07	2.6E-04	1.7E-08	1.2E-04
NGC 3384		1.1E+07	5	4.4E+39	6	143.0	1	28.4	1.4	2.0E+10	1	1.4	1.1E-02	1.2E-06	3.7E-05	1.0E-09	6.7E-05
NGC 3393	Seyfert	1.6E+07	5	2.7E+42	49	184.0	1	28.5	6.8	1.0E+11	1	4.3	1.6E-02	2.2E-04	5.3E-05	1.5E-09	4.7E-05
NGC 3414		2.5E+08	7	1.3E+41	50	205.0	1	63.5	3.2	5.0E+10	1	1.7	5.1E-02	6.3E-06	3.1E-04	2.4E-08	1.6E-04
NGC 3489	Seyfert	5.9E+06	5	1.0E+40	5	129.0	37	20.0	1.7	3.8E+10	37	3.3	1.2E-02	7.3E-06	3.1E-05	5.7E-10	2.1E-05

Table A1 (cont'd)

Galaxy Name	Type	M_B ($M_\odot$)	Ref.	L_B (erg/s)	Ref.	σ_b (km/s)	Ref.	σ_B (km/s)	σ_p (km/s)	M_b ($M_\odot$)	Ref.	r_b (kpc)	r_B (kpc)	r_p (kpc)	r_x (kpc)	r_s (kpc)	ε_b (m^2/s^3)
NGC 3557				7.8E+41	63	264.1	63		5.0	5.8E+11	63	12.0		8.1E-05			5.0E-05
NGC 3585		3.3E+08	5	1.5E+40	2	213.0	1	53.9	1.9	1.8E+11	1	5.7	9.3E-02	3.8E-06	5.0E-04	3.2E-08	5.5E-05
NGC 3607		1.4E+08	5	6.3E+39	2	229.0	1	49.8	1.5	1.6E+11	1	4.4	4.5E-02	1.2E-06	2.3E-04	1.3E-08	8.9E-05
NGC 3608	LINER	4.7E+08	5	9.7E+39	2	182.0	1	55.9	1.7	9.7E+10	1	4.2	1.2E-01	3.3E-06	6.8E-04	4.5E-08	4.6E-05
NGC 3665		5.8E+08	59	1.7E+41	59	219.0	59	60.1	3.4	2.1E+11	59	6.3	1.3E-01	2.4E-05	7.6E-04	5.5E-08	5.4E-05
NGC 3842	BCG	9.1E+09	5	1.3E+42	59	270.0	23	86.3	5.7	1.6E+12	23	30.6	1.0E+00	2.8E-04	7.7E-03	8.7E-07	2.1E-05
NGC 3862		2.6E+08	59	5.8E+41	59	209.0	59	43.8	4.6	3.6E+11	59	11.9	1.1E-01	1.3E-04	5.1E-04	2.5E-08	2.5E-05
NGC 3923				7.9E+41	63	246.6	63		5.0	4.2E+11	63	10.0		8.5E-05			4.8E-05
NGC 3945		8.8E+06	5	5.6E+40	5	182.0	24	39.8	2.6	1.0E+10	24	0.4	4.5E-03	1.2E-06	2.0E-05	8.5E-10	4.5E-04
NGC 3955				3.3E+40	63	94.4	63		2.3	1.4E+10	63	2.2		3.0E-05			1.2E-05
NGC 3982	Seyfert	8.0E+07	5	9.5E+41	60	78.0	44	26.0	5.2	1.1E+10	45	2.6	9.7E-02	7.9E-04	3.0E-04	7.7E-09	5.9E-06
NGC 3998	Seyfert	8.5E+08	5	4.4E+42	2	305.0	1	118.2	7.7	5.5E+10	1	0.9	5.0E-02	1.4E-05	4.8E-04	8.1E-08	1.1E-03
NGC 4026		1.8E+08	5	5.4E+39	2	180.0	1	51.8	1.4	5.2E+10	1	2.3	5.5E-02	1.2E-06	2.9E-04	1.7E-08	8.2E-05
NGC 4036	LINER	7.7E+07	59	3.0E+40	59	182.0	59	42.6	2.2	6.2E+10	59	2.7	3.5E-02	4.8E-06	1.6E-04	7.4E-09	7.2E-05
NGC 4041	Seyfert	6.4E+06	5	1.7E+40	51	95.0	25	25.7	1.9	2.5E+09	25	0.4	7.9E-03	3.3E-06	2.5E-05	6.1E-10	7.0E-05
NGC 4073				3.6E+43	63	267.0	63		13.0	1.0E+12	63	20.8		2.4E-03			3.0E-05
NGC 4104				1.2E+43	63	291.0	63		9.8	1.6E+12	63	26.4		1.0E-03			3.0E-05
NGC 4125				2.5E+41	63	238.2	63		3.8	2.5E+11	63	6.4		2.5E-05			6.8E-05
NGC 4143	LINER	1.4E+08	5	1.4E+41	5	271.0	27	66.0	3.3	9.3E+10	29	1.8	2.6E-02	3.2E-06	1.7E-04	1.3E-08	3.5E-04
NGC 4151	Seyfert	4.5E+07	2	7.7E+42	2	93.0	1	28.1	8.9	1.0E+10	1	1.7	4.6E-02	1.4E-03	1.5E-04	4.3E-09	1.6E-05
NGC 4203	LINER	3.8E+07	5	4.0E+41	5	110.0	27	28.8	4.2	1.8E+10	29	2.1	3.7E-02	1.2E-04	1.3E-04	3.7E-09	2.1E-05
NGC 4258	Seyfert	3.8E+07	5	1.1E+42	2	115.0	1	33.0	5.4	1.1E+10	1	1.2	2.8E-02	1.2E-04	1.1E-04	3.6E-09	4.1E-05
NGC 4261	LINER	5.3E+08	5	5.2E+41	3a	315.0	1	76.3	4.5	3.6E+11	1	5.2	7.4E-02	1.5E-05	5.2E-04	5.1E-08	1.9E-04
NGC 4278	LINER	6.6E+08	3	4.7E+41	3a	232.5	31	77.7	4.4	9.0E+10	29	2.4	9.0E-02	1.6E-05	6.4E-04	6.3E-08	1.7E-04
NGC 4291	BCG	9.8E+08	5	1.6E+40	6	242.0	1	81.3	1.9	1.3E+11	1	3.2	1.2E-01	1.5E-06	8.9E-04	9.4E-08	1.4E-04
NGC 4303	Seyfert	4.5E+06	2	1.2E+40	2	84.0	1	23.1	1.8	1.6E+09	1	0.3	6.8E-03	3.0E-06	2.0E-05	4.3E-10	5.9E-05
NGC 4321		2.7E+07	5	2.7E+39	5	69.0	18	21.1	1.2	5.8E+09	18	1.8	5.0E-02	9.4E-06	1.3E-04	2.6E-09	6.1E-06
NGC 4342		4.5E+08	5	2.1E+40	2	225.0	1	104.3	2.0	1.2E+10	1	0.3	3.4E-02	2.5E-07	3.0E-04	4.4E-08	1.1E-03
NGC 4365				6.5E+40	63	246.9	63		2.7	2.4E+11	63	5.6		7.2E-06			8.7E-05
NGC 4374	Seyfert	9.3E+08	5	6.1E+40	3a	296.0	1	80.2	2.6	3.6E+11	1	5.9	1.2E-01	4.2E-06	8.6E-04	8.9E-08	1.4E-04
NGC 4382		1.3E+07	5	5.7E+39	5	182.0	38	21.4	1.5	3.3E+11	38	14.4	2.3E-02	7.4E-06	6.3E-05	1.2E-09	1.4E-05
NGC 4388	Seyfert	7.3E+06	5	4.2E+42	5	107.0	1	24.8	7.6	6.2E+09	1	0.8	9.7E-03	2.8E-04	2.9E-05	7.0E-10	5.1E-05
NGC 4406				1.6E+42	63	230.0	63		6.0	2.6E+11	63	7.0		1.2E-04			5.6E-05
NGC 4435		8.0E+06	5	6.2E+40	61	156.0	26	30.7	2.6	1.5E+10	26	0.9	6.9E-03	4.4E-06	2.5E-05	7.7E-10	1.4E-04
NGC 4438	LINER	5.6E+07	3	1.2E+40	3a	142.0	39	56.2	1.8	3.3E+09	39	0.2	1.5E-02	4.6E-07	8.1E-05	5.4E-09	3.9E-04
NGC 4457				8.5E+40	63	113.3	63		2.9	3.2E+10	63	3.6		5.9E-05			1.3E-05
NGC 4459	HII	7.0E+07	5	1.3E+40	6	167.0	1	36.5	1.8	7.9E+10	1	4.1	4.3E-02	5.0E-06	1.7E-04	6.7E-09	3.7E-05
NGC 4472	Seyfert	2.5E+09	3	3.2E+40	62	250.0	40	83.7	2.2	3.4E+11	29	7.8	2.9E-01	5.6E-06	2.2E-03	2.4E-07	6.5E-05
NGC 4473		9.0E+07	5	5.0E+39	2	190.0	1	42.4	1.4	9.2E+10	1	3.7	4.1E-02	1.5E-06	1.8E-04	8.6E-09	6.1E-05
NGC 4477	Seyfert	8.4E+07	5	1.6E+41	63	144.8	31	36.8	3.4	4.5E+10	29	3.1	5.1E-02	3.8E-05	2.1E-04	8.1E-09	3.2E-05
NGC 4486		6.2E+09	5	9.3E+41	3a	375.0	1	134.0	5.2	6.0E+11	1	6.1	2.8E-01	1.7E-05	3.0E-03	5.9E-07	2.8E-04
NGC 4486A		1.4E+07	5	2.2E+39	6	111.0	1	32.0	1.2	4.1E+09	1	0.5	1.2E-02	5.4E-07	4.2E-05	1.4E-09	9.2E-05
NGC 4486B		6.0E+08	5	1.5E+39	5	169.8	47	97.0	1.0	5.6E+09	47	0.3	5.2E-02	6.5E-08	4.4E-04	5.8E-08	5.7E-04
NGC 4501	Seyfert	7.9E+07	5	2.4E+40	5	130.0	21	41.9	2.1	1.3E+10	21	1.1	3.7E-02	4.6E-06	1.6E-04	7.6E-09	6.5E-05
NGC 4526		4.5E+08	5	3.1E+40	5	195.4	31	60.0	2.2	9.4E+10	29	3.5	1.0E-01	5.3E-06	6.0E-04	4.3E-08	6.8E-05
NGC 4548	LINER	3.4E+07	5	2.4E+41	5	143.7	31	42.3	3.7	8.7E+09	43	0.6	1.6E-02	1.0E-05	7.0E-05	3.3E-09	1.6E-04
NGC 4552	LINER	5.0E+08	1	2.5E+40	3a	252.0	1	76.5	2.1	1.1E+11	1	2.5	7.0E-02	1.4E-06	4.9E-04	4.8E-08	2.1E-04
NGC 4555				2.7E+42	63	344.0	63		6.8	1.0E+12	63	12.6		9.7E-05			1.0E-04
NGC 4564		8.8E+07	5	9.7E+39	2	162.0	1	41.8	1.7	4.4E+10	1	2.4	4.1E-02	2.6E-06	1.8E-04	8.5E-09	5.7E-05
NGC 4594	LINER	6.7E+08	5	1.9E+41	3a	240.0	1	64.5	3.5	2.7E+11	1	6.8	1.3E-01	2.1E-05	8.1E-04	6.4E-08	6.6E-05
NGC 4596		7.7E+07	5	2.4E+39	6	136.0	1	37.9	1.2	2.6E+10	1	2.0	4.4E-02	1.3E-06	1.8E-04	7.4E-09	4.0E-05
NGC 4621		4.0E+08	1	1.0E+39	53	211.0	1	73.6	1.0	4.4E+10	1	1.4	6.0E-02	1.3E-07	4.1E-04	3.8E-08	2.1E-04
NGC 4636	LINER	3.1E+08	3	2.9E+40	3a	174.3	31	73.7	2.2	1.3E+10	29	0.6	4.7E-02	1.2E-06	3.2E-04	3.0E-08	2.8E-04
NGC 4649		4.7E+09	5	7.0E+39	3a	385.0	1	135.9	1.5	4.9E+11	1	4.8	2.1E-01	3.0E-07	2.3E-03	4.5E-07	3.9E-04
NGC 4696	BCG	7.2E+08	3	2.4E+39	3a	251.2	37	57.1	1.2	6.8E+11	37	15.5	1.8E-01	1.6E-06	1.0E-03	7.0E-08	3.3E-05
NGC 4697	BCG	2.0E+08	5	7.2E+39	3a	177.0	1	44.8	1.5	1.1E+11	1	5.1	8.2E-02	3.4E-06	3.9E-04	1.9E-08	3.6E-05
NGC 4710				1.6E+40	63	116.5	63		1.9	3.2E+10	63	3.4		1.4E-05			1.5E-05
NGC 4742		1.4E+07	5	1.1E+40	6	90.0	1	23.8	1.7	6.2E+09	1	1.1	2.0E-02	7.9E-06	5.9E-05	1.3E-09	2.1E-05
NGC 4751		2.4E+09	5	2.6E+40	5	355.0	42	123.2	2.1	2.8E+11	42	3.1	1.3E-01	6.9E-07	1.3E-03	2.3E-07	4.6E-04
NGC 4782				1.9E+42	63	308.5	63		6.2	8.5E+11	63	12.8	0.0E+00	1.0E-04			7.4E-05
NGC 4826	Seyfert	1.6E+06	5	7.8E+38	5	126.0	21	24.0	0.9	3.5E+09	21	0.3	2.2E-03	1.1E-07	6.5E-06	1.5E-10	2.0E-04
NGC 4889		2.1E+10	5	5.2E+41	5	347.0	17	137.0	4.5	1.2E+12	17	14.7	9.1E-01	3.2E-05	9.9E-03	2.0E-06	9.2E-05
NGC 4936				1.9E+42	63	278.2	63		6.2	8.0E+11	63	14.8		1.6E-04			4.7E-05
NGC 4945	Seyfert	1.4E+06	5	1.0E+39	2	134.0	1	25.6	0.9	3.0E+09	1	0.2	1.7E-03	8.4E-08	5.2E-06	1.3E-10	3.2E-04
NGC 5005		1.6E+08	3	2.5E+41	3a	139.0	18	45.3	3.8	2.5E+10	18	1.8	6.3E-02	3.6E-05	3.0E-04	1.5E-08	4.7E-05
NGC 5018				2.4E+41	63	206.5	63		3.7	2.3E+11	63	7.8		4.6E-05			3.7E-05
NGC 5044	BCG	5.1E+08	3	2.6E+40	3a	239.9	37	52.9	2.1	5.6E+11	37	14.0	1.5E-01	9.8E-06	8.0E-04	4.9E-08	3.2E-05
NGC 5077	BCG	8.6E+08	5	1.1E+41	6	222.0	1	65.9	3.0	2.1E+11	1	6.1	1.6E-01	1.6E-05	1.0E-03	8.2E-08	5.8E-05
NGC 5128	Seyfert	5.7E+07	5	2.6E+41	2	150.0	1	36.9	3.8	3.6E+10	1	2.3	3.4E-02	3.8E-05	1.4E-04	5.5E-09	4.7E-05
NGC 5252	Seyfert	1.0E+09	2	2.5E+44	2	190.0	1	56.7	21.1	2.4E+11	1	9.6	2.5E-01	1.3E-02	1.4E-03	9.6E-08	2.3E-05
NGC 5328	BCG	4.7E+09	59	2.7E+42	59	331.0	59	109.9	6.8	6.6E+11	59	8.7	3.2E-01	7.5E-05	2.9E-03	4.5E-07	1.4E-04
NGC 5353				6.9E+41	63	283.5	63		4.8	3.6E+11	63	6.4		3.2E-05			1.2E-04

Table A1 (cont'd)

Galaxy Name	Type	M_B ($M_\odot$)	Ref.	L_B (erg/s)	Ref.	σ_b (km/s)	Ref.	σ_B (km/s)	σ_p (km/s)	M_b ($M_\odot$)	Ref.	r_b (kpc)	r_B (kpc)	r_p (kpc)	r_x (kpc)	r_s (kpc)	ε_b (m^2/s^3)
NGC 5419	BCG	7.2E+09	59	5.0E+42	59	367.0	59	110.0	7.9	1.7E+12	59	18.2	4.9E-01	1.8E-04	4.5E-03	7.0E-07	8.8E-05
NGC 5490	BCG	5.4E+08	59	1.3E+42	59	257.0	59	68.3	5.7	2.3E+11	59	5.0	9.4E-02	5.5E-05	6.1E-04	5.2E-08	1.1E-04
NGC 5516		3.7E+09	5			328.2	35	111.7		4.6E+11	35	6.2	2.4E-01		2.3E-03	3.5E-07	1.9E-04
NGC 5532				2.8E+42	63	277.8	63		6.9	7.8E+11	63	14.6		2.2E-04			4.8E-05
NGC 5576		2.7E+08	5	4.1E+39	6	183.0	1	46.3	1.3	1.5E+11	1	6.5	1.0E-01	2.6E-06	5.0E-04	2.6E-08	3.1E-05
NGC 5643	Seyfert	2.8E+06	34	1.0E+43	19	130.0	34	25.4	9.5	5.5E+09	34	0.5	3.5E-03	1.8E-04	1.1E-05	2.6E-10	1.5E-04
NGC 5813	LINER	7.1E+08	1	7.3E+39	3a	230.0	1	74.9	1.6	1.1E+11	1	3.0	1.0E-01	9.2E-07	7.2E-04	6.8E-08	1.3E-04
NGC 5845		4.9E+08	5	1.9E+40	2	234.0	1	87.9	2.0	3.7E+10	1	1.0	5.2E-02	5.7E-07	4.0E-04	4.7E-08	4.3E-04
NGC 5846	BCG	1.1E+09	7	9.2E+40	3a	238.0	1	67.1	2.9	3.5E+11	1	8.9	2.0E-01	1.6E-05	1.3E-03	1.1E-07	4.9E-05
NGC 5866				5.2E+40	63	161.6	63		2.5	9.4E+10	63	5.2		2.0E-05			2.6E-05
NGC 6086	BCG	3.7E+09	5			318.0	32	86.8		1.4E+12	32	19.9	4.1E-01		3.1E-03	3.6E-07	5.2E-05
NGC 6098				3.1E+42	63	275.3	63		7.0	1.1E+12	63	21.6		3.6E-04			3.1E-05
NGC 6107				7.3E+42	63	240.9	63		8.7	1.3E+12	63	31.2		1.5E-03			1.5E-05
NGC 6166		1.9E+09	3	2.7E+41	3a	302.0	33	62.4	3.8	2.8E+12	33	44.2	3.9E-01	9.0E-05	2.4E-03	1.8E-07	2.0E-05
NGC 6251	Seyfert	6.1E+08	5	5.0E+43	2	290.0	1	66.3	14.1	5.6E+11	1	9.6	1.1E-01	1.1E-03	7.2E-04	5.9E-08	8.2E-05
NGC 6264	Seyfert	3.1E+07	5	1.3E+42	65	158.0	1	40.4	5.6	1.6E+10	1	0.9	1.5E-02	4.2E-05	6.7E-05	3.0E-09	1.4E-04
NGC 6269				1.3E+43	63	317.9	63		10.2	1.3E+12	63	18.2		5.9E-04			5.7E-05
NGC 6278				2.1E+41	63	193.2	63		3.6	1.4E+11	63	5.4		3.5E-05			4.3E-05
NGC 6323		1.0E+07	5	8.7E+43	56a	158.0	1	35.5	16.2	1.0E+10	1	0.6	6.6E-03	6.3E-04	2.6E-05	9.7E-10	2.2E-04
NGC 6338				4.2E+43	63	348.4	63		13.5	2.1E+12	63	24.8		1.4E-03			5.5E-05
NGC 6482				1.0E+43	63	316.8	63		9.5	5.2E+11	63	7.4		2.0E-04			1.4E-04
NGC 6861		2.1E+09	5	1.8E+40	5	388.8	35	134.0	1.9	2.5E+11	35	2.3	9.6E-02	2.9E-07	1.0E-03	2.0E-07	8.2E-04
NGC 6868				1.3E+42	63	250.1	63		5.7	5.4E+11	63	12.4	0.0E+00	1.5E-04			4.1E-05
NGC 7052		4.0E+08	5	7.7E+41	2	266.0	1	63.5	5.0	2.9E+11	1	5.9	8.0E-02	3.9E-05	4.9E-04	3.8E-08	1.0E-04
NGC 7176				4.0E+41	63	245.9	63		4.2	5.0E+11	63	12.0		6.1E-05			4.0E-05
NGC 7196				7.6E+41	63	277.9	63		5.0	4.2E+11	63	7.8		4.4E-05			8.9E-05
NGC 7332		1.3E+07	8	1.7E+39	54	122.0	8	26.6	1.1	1.5E+10	8	1.5	1.5E-02	1.0E-06	4.8E-05	1.2E-09	4.1E-05
NGC 7457	Galaxy	9.0E+06	5	1.6E+39	6	67.0	1	15.8	1.1	7.0E+09	1	2.2	2.9E-02	8.9E-06	6.4E-05	8.6E-10	4.3E-06
NGC 7582	Seyfert	5.5E+07	5	3.2E+43	19a	156.0	1	29.5	12.6	1.3E+11	1	7.7	5.2E-02	4.1E-03	1.8E-04	5.3E-09	1.6E-05
NGC 7618				9.4E+42	63	292.8	63		9.3	9.4E+11	63	15.8		5.1E-04			5.1E-05
NGC 7619	BCG	2.3E+09	5	2.0E+42	59	292.0	17	90.9	6.3	4.5E+11	17	7.5	2.3E-01	7.5E-05	1.8E-03	2.2E-07	1.1E-04
NGC 7626		3.8E+08	59	6.2E+41	59	234.0	59	55.8	4.7	2.8E+11	59	7.4	1.0E-01	6.0E-05	5.5E-04	3.7E-08	5.6E-05
NGC 7768	BCG	1.3E+09	5			257.0	36	68.4		5.7E+11	36	12.4	2.3E-01		1.5E-03	1.3E-07	4.4E-05
UGC 408				1.2E+42	63	197.6	63		5.6	3.1E+11	63	11.4		2.6E-04			2.2E-05
UGC 1841	Seyfert	3.0E+08	59	6.6E+42	59	295.0	59	45.7	8.5	1.9E+12	59	31.0	1.2E-01	7.5E-04	5.5E-04	2.8E-08	2.7E-05
Mrk 1216	LINER	4.9E+09	59	4.4E+42	59	324.1	59	172.1	7.7	6.6E+10	59	0.9	1.4E-01	1.2E-05	1.7E-03	4.7E-07	1.2E-03

[a]BH bolometric luminosity L_B directly provided by the reference in column (6). Otherwise (without 'a'), L_B was estimated using the X-ray luminosity in the 2-10 kev band, i.e. $L_B = L_{2-10} \times 15.8$ (Ho 2009).

References. — (1) Benedetto et al. 2013; (2) Gultekin et al. 2009b; (3) Inayoshi et al. 2020; (4) Zhang et al. 2009; (5) Gultekin et al. 2019; (6) Gultekin et al. 2012; (7) Hu 2008; (8) Haring & Rix 2004; (9) Marconi & Hunt 2003; (10) McConnell & Ma 2013; (11) Boizelle et al. 2021; (12) Bettoni et al. 2003; (13) McConnachie 2012; (14) van den Bosch et al. 2012; (15) Rusli et al. 2011; (16) Spolaor et al. 2008; (17) Bogdan et al. 2018; (18) Das et al. 2003; (19 Brightman et al. 2017; (20) Marin 2016; (21) Davis et al. 2019; (22) Bennert et al. 2006; (23) Benedetto et al. 2013; (24) Dullo et al. 2016; (25) Marconi et al. 2003; (26) Coccato et al. 2006; (27) Sarzi et al. 2002; (28) Fisher & Drory 2010; (29 Cappellari et al. 2011; (30) Cappellari et al. 2013; (31) Beifiori et al. 2012; (32) McConnell et al. 2011; (33) Bender et al. 2015; (34) Garcia-Bernete et al. 2021; (35) Rusli et al. 2013; (36) McConnell et al. 2012; (37) Samir et al. 2016; (38) Gultekin et al. 2011; (39) Perez et al. 2009; (40) Chae et al. 2018; (41) Sahu et al. 2019; (42) Lakhchaura et al. 2019; (43) Weinzirl et al. 2009; (44) Beifiori et al. 2009; (45) Sanchez-Portal et al. 2004; (46) Ho et al. 2009; (47) Samir et al. 2016; (48) Burtscher et al. 2015; (49) Koss et al. 2015; (50) Gonzalez-Martin et al. 2009; (51) Williams et al. 2022; (52) Gao et al. 2017; (53) Wrobel et al. 2008; (54) Nagar et al. 2005; (55) Fabian et al. 2013; (56) Kuo et al. 2020; (57) Swartz et al. 2006; (58) Urquhart et al. 2022; (59) Lakhchaura et al. 2019; (60) Kammoun et al. 2020; (61) Machacek et al. 2004; (62) Maccarone et al. 2011; (63) Babyk et al. 2018; (64) Gultekin et al. 2009a; (65) Castangia et al. 2013;

Note. — This table lists the SMBH and host galaxy data used in our co-evolution analysis. Columns list galaxy name, galaxy type (from SIMBAD astronomical database), the BH mass M_B, the estimated BH Bolometric luminosity L_B, the bulge velocity dispersion σ_b, the bulge mass M_b. The five length scales are computed quantities from these data, i.e. the bulge size $r_b = GM_b/(3\sigma_b^2)$ (Marconi & Hunt 2003), the BH sphere of influence r_B (Eq. (15)), the radiation scale r_p (Eq. (16)), the dissipation scale r_x (Eq. (17)), and the Schwarzschild radius r_s (Eq. (15)). The rate of energy cascade can be estimated as $\varepsilon_b = \sigma_b^3/r_b$. Velocity dispersions on scales r_B and r_p are also presented as σ_B and σ_p (Fig. 4).